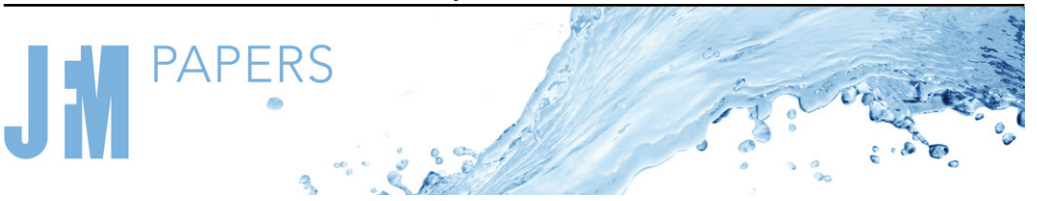
J. Fluid Mech. (2025), *vol.* 1010, A5, doi:10.1017/jfm.2025.283



Optimal Strouhal numbers for oscillatory propulsion in density stratified fluids

Jiadong Wang[1], **Prabal Kandel**[1] **and Jian Deng**[1]

[1]State Key Laboratory of Fluid Power and Mechatronic Systems, Department of Mechanics, Zhejiang University, Hangzhou 310027, PR China

Corresponding author: Jian Deng, zjudengjian@zju.edu.cn

(Received 4 September 2024; revised 4 March 2025; accepted 7 March 2025)

The propulsive efficiency of flying and swimming animals propelled by oscillatory appendages typically peaks within a narrow Strouhal number range of $0.20 < St < 0.40$. Motivated by the ubiquitous presence of stratification in natural environments, we numerically investigate the optimal Strouhal numbers St_m for an oscillating foil in density stratified fluids. Our results reveal that St_m increases with the strength of stratification characterised by the internal Froude number Fr, giving rise to markedly higher values under strong stratifications compared with those observed in homogeneous fluids. The propulsive efficiency tends to maximise when there is a resonance between the oscillations of the foil and the fluid, as inferred from a fitted line in the (St, Fr) parameter space, which shows that St_m is proportional to Fr^{-1}. We further uncover that the significant increase in St_m in strongly stratified regimes is fundamentally driven by fluid entrainment. During this process, the oscillating foil induces perturbations in the density field, resulting in buoyancy-driven restoring forces which alter the pressure distribution on the foil and thus the hydrodynamic forces. Notably, only under strongly stratified conditions, where dominant buoyancy effects confine the density transport to the vicinity of the oscillating foil, the intensified density perturbation due to the increase in St can be effectively harnessed to enhance thrust production, thereby contributing to the elevated St_m. These insights suggest that oscillatory propulsors should adopt new kinematic strategies involving relatively large Strouhal numbers to achieve efficient cruising in strongly stratified environments.

Key words: propulsion, swimming/flying, stratified flows

1. Introduction

Through long-term natural selection, flying and swimming animals that use oscillatory propulsion have evolved the ability to move with remarkably high efficiency. A critical dimensionless parameter that links propulsive performance to kinematics of tails and

© The Author(s), 2025. Published by Cambridge University Press.

https://doi.org/10.1017/jfm.2025.283 Published online by Cambridge University Press

wings is the Strouhal number (St), defined as the product of oscillatory frequency and stroke amplitude divided by the moving speed. Observational data indicate that fish and cetaceans typically achieve the optimum propulsion within a narrow St range of 0.25–0.35 (Triantafyllou *et al.* 1991, 1993, 2000). Further investigations by Rohr & Fish (2004), examining the locomotion of seven species of odontocete cetaceans over a broad range of forward speeds, confirmed that most cetaceans prefer swimming at St values between 0.20 and 0.40. Similarly, Eloy (2012) conducted a comprehensive analysis of the swimming kinematics of 53 species of aquatic animals, reporting an analogous optimal range for St in oscillatory-based swimmers. Despite variations in swimming speed and body size, the optimal St range of $0.20 < St < 0.40$ is conserved across different Reynolds numbers according to these observations. More interestingly, Nudds *et al.* (2014) found that fish can maintain their preferred St values through a trade-off between tail beat frequency and peak-to-peak stroke amplitude, even when water temperature changes, suggesting a consistent occurrence of optimal St in fish swimming. By analogy, Taylor *et al.* (2003) analysed the Strouhal numbers of 42 species of birds, bats and insects, discovering that the optimal St range for flying animals also converges within the interval of 0.20–0.40. Thus, optimising Strouhal numbers into this constrained range by tuning swimming and flying kinematics appears to be a general principle for animals employing oscillatory propulsion to achieve efficient cruising. In addition, Gazzola *et al.* (2014) examined the existing locomotion data spanning a large number of aquatic swimmers and discovered the same converging behaviour of Strouhal number as the above findings. Especially, they derived a scaling relation that links cruising speed to body kinematics and fluid properties, which provides a physical basis for the observations that swimming and flying animals commonly operate within a narrow St range.

The growing interest in efficient cruising of animals has inspired the development of innovative propulsion systems for both autonomous underwater vehicles and micro air vehicles. An oscillating foil, undergoing combined heaving and pitching motion with a specific phase difference, serves as an effective analogy to natural oscillatory fins and wings. Anderson *et al.* (1998) and Read *et al.* (2003) conducted a number of experimental measurements on the propulsive performance of an isolated oscillating foil, and found that significantly high efficiency can be attained by an appropriate combination of kinematic and geometric parameters. Notably, they indicated that the efficiency of a harmonically heaving and pitching foil tends to peak within the St range of 0.20–0.40, consistent with biological observations. Inspired by the pectoral fins of aquatic animals, Techet (2008) experimentally measured the propulsive performance of a three-dimensional rolling and pitching foil at high Reynolds numbers. He also observed the optimum efficiency within the interval $0.20 < St < 0.40$, with a maximum efficiency at $St = 0.30$. Using an idealised model of an elliptical foil subjected to vertical oscillation, Deng & Caulfield (2016, 2018) observed that the foil transitions into a self-propelled state, achieving nearly constant horizontal speeds after symmetry breaking occurs. The resulting Strouhal numbers fall within the range of 0.32–0.40 for two-dimensional cases and 0.25–0.35 for three-dimensional cases (oblate spheroids) when the aspect ratio is less than 0.4. Floryan *et al.* (2017) and Van Buren *et al.* (2019) employed the comprehensive propulsive data to propose new scaling laws for thrust, power and efficiency of oscillating foils. When plotted as a function of Strouhal number, the maximum efficiency tends to converge on the optimal range $0.20 < St < 0.40$, whether for purely heaving/pitching foils or oscillating foils in combined heaving and pitching motion. These findings are further supported by extensive theoretical analyses and numerical simulations (Guglielmini & Blondeaux 2004; Young & Lai 2007; Lua *et al.* 2016; Şentürk & Smits 2019),

https://doi.org/10.1017/jfm.2025.283 Published online by Cambridge University Press

indicating that the Strouhal number must be tightly constrained to achieve efficient propulsion.

The following question then arises. Why does optimum efficiency consistently occur within the range of $0.20 < St < 0.40$ for both biological appendages and artificial foils? A stability analysis by Triantafyllou *et al.* (1991, 1993) indicated that the average velocity profile in the wake of an oscillating foil exhibits a jet pattern, which becomes convectively unstable over a narrow range of frequencies corresponding to this optimal St interval. They proposed that optimum efficiency is achieved within this specific Strouhal number range because the oscillatory frequency of the foils coincides with the frequency of maximum spatial amplification of disturbances. From an aerodynamic or hydrodynamic perspective, the viscous effects play a significant role and thus the drag dominates the streamwise force when foils perform weak motion at low Strouhal numbers, resulting in poor efficiency (Smits 2019). As the Strouhal number increases, the influence of drag force becomes weaker. Established scaling laws for the propulsive performance of oscillating foils, derived from circulatory and added mass forces, indicate that both the thrust production and power expenditure increase nonlinearly with St, leading to a rapid rise in efficiency to a peak at a specific St value, followed by a mild decline (Floryan *et al.* 2017; Van Buren *et al.* 2019). Given that the maximum angle of attack is determined by the Strouhal number, a strong foil motion at extremely high St may induce large-scale flow separation and dynamic stall behaviours, significantly reducing propulsive efficiency (Isogai *et al.* 1999; Tuncer & Kaya 2005; Young & Lai 2007). Additionally, the optimal frequency of oscillating foils was thought to be selected by intrinsic time scales associated with vortex growth and leading-edge vortex shedding (Wang 2000), suggesting that the Strouhal numbers are inherently related to propulsive performance.

Owing to tremendous efforts, the understandings of oscillatory swimming and newly developed propulsion systems inspired by natural swimmers have reached an encouraging level (Rozhdestvensky & Ryzhov 2003; Platzer *et al.* 2008; Wu 2011; Smits 2019). The literature in this field spans a broad range of aspects, including performance optimisation (Tuncer & Kaya 2005; Izraelevitz & Triantafyllou 2014), the roles of flexibility (Zhu 2007; Alben 2008), flow structure manipulation (Liao *et al.* 2003; Fish & Lauder 2006), three-dimensional effects (Dong *et al.* 2006; Buchholz & Smits 2008) and the characteristics of multi-foil arrangements (Muscutt *et al.* 2017; Alben 2021). However, existing studies on oscillatory propulsion have mostly focused on homogeneous environments. In reality, oceans are inherently stratified in density due to variations in temperature, salinity and pressure with depth (Thorpe 2005). Especially for the upper layer of the ocean where the density gradient is notably high, known as pycnocline, stratification effects play an important role in the locomotion and hydrodynamics of swimmers (More & Ardekani 2023). Despite the oceanic density gradient covering a large spatial scale, the fundamental length scale that dictates stratification effects on the motion of marine swimmers was found to be much smaller and comparable with that of biological activity (Ardekani & Stocker 2010). The significant role of density stratification has been identified in many physical processes, ranging from wake evolution of metre-scale objects (Spedding 2014) to settling dynamics of centimetre-scale zooplankton (Magnaudet & Mercier 2020). It is therefore anticipated that either natural oscillatory swimmers, such as fish and mammals (Gazzola *et al.* 2014), or man-made devices, such as underwater vehicles and gliders equipped with oscillating wings (Zhou & Low 2011; Rozhdestvensky 2022), will exhibit distinct dynamical behaviours in stratified environments with a sufficiently large density gradient when compared with homogeneous observations. This raises the following crucial question. What are the preferred Strouhal numbers for oscillatory propulsion in a density stratified fluid? Our study aims to address this question.

https://doi.org/10.1017/jfm.2025.283 Published online by Cambridge University Press

Fluid parcels displaced vertically in a stratified environment experience a buoyancy-driven restoring force, leading to distinctive phenomena that challenge the mechanisms and principles established in homogeneous fluids. The literature on the interaction between density stratification and structures covers a wide range of topics. One of the most prominent features in a stably stratified fluid is the triggering of internal waves, which plays a crucial role in mass and momentum transport in oceans (Sutherland 2010). Early studies primarily focused on modelling and measuring internal wave dynamics (Hurley & Keady 1997; Flynn *et al.* 2003), significantly advancing our understanding of their generation and propagation mechanisms. More recent research has increasingly focused on nonlinear effects, such as wave–flow interactions, wave breaking events and energy transfer (Allshouse *et al.* 2016; Howland *et al.* 2021). In addition, wake dynamics of bodies with varying shapes in stratified fluids have garnered significant attention. Early efforts can be traced back to the studies on the evolution of vortices generated by either two- or three-dimensional wings in a stratified fluid (Sarpkaya 1983; Spalart 1996). By revealing the leading mechanisms governing the rise, demise and trajectory of the vortices, these works enhance the comprehension into the interaction of aircraft wakes and stratified atmospheres, and thus offer important implications for air traffic control. For bluff bodies in horizontal motion, the wakes are characterised by the persistence of coherent structures with a high horizontal–vertical length ratio due to the inhibition of vertical motion (Spedding *et al.* 1996; Meunier & Spedding 2006). Madison *et al.* (2022) further indicated that the wake structures of a body towed at a constant horizontal speed can be categorised into different flow regimes, depending on the relative contributions of inertial, buoyancy and viscous effects. In the case of a sphere moving vertically at a constant speed, the flow pattern was shown to exhibit a strong rear jet due to the complete collapse of the axisymmetric standing vortex under stratification effects (Torres *et al.* 2000; Okino *et al.* 2017).

Considerable research has also been devoted to the dynamics of freely moving bodies in a stratified fluid. Doostmohammadi *et al.* (2014) reported that the settling dynamics of a sphere can be influenced significantly by the presence of stratification. They observed an oscillation in settling velocity and even levitation behaviour after the sphere reaches peak speed. Lam *et al.* (2019) examined the fluttering behaviour of rigid discs falling freely in stably stratified fluids, and found that density stratification tends to increase radial dispersion while greatly reducing peak inclination angle, fluttering amplitude and vertical descent velocity. More & Ardekani (2020) investigated the influence of density stratification on the self-propulsion characteristics of a squirmer, noting that a pusher propelling from the rear is a more efficient swimmer than a puller propelling from the front due to more efficient advection of vorticity downstream. These studies provide valuable insights into the contribution of swimming organisms and sedimenting particles to the mixing process in oceans and lakes (Ardekani *et al.* 2017; Houghton *et al.* 2018).

In contrast to the extensive research on stratification-induced alteration of flow structures, relatively few studies have focused on the hydrodynamic forces acting on submersed bodies in stratified fluids. Lofquist & Purtell (1984) and Arntsen (1996) examined the drag force of bluff bodies moving horizontally in stably stratified fluids and reported an evident sensitivity of the drag coefficient to the strength of stratification. Additionally, Ermanyuk & Gavrilov (2002, 2003) explored the hydrodynamic loads on both two-dimensional circular cylinders and three-dimensional spheres oscillating horizontally under stratification conditions, revealing a clear dependence of added mass and damping coefficients on the vertical extent of stratification. These findings suggest that the force characteristics of bodies in stratified fluids differ both qualitatively and quantitatively from those in homogeneous fluids. Nonetheless, the physical mechanisms

https://doi.org/10.1017/jfm.2025.283 Published online by Cambridge University Press

underlying such differences in force and moment, particularly for swimmers with a complex motion mode, remain inadequately understood.

Our previous study (Wang *et al.* 2024) has evaluated the hydrodynamic performance of a combined heaving and pitching foil at a constant Strouhal number, finding that both thrust production and propulsive efficiency are enhanced through the proper resonance between foil kinematics and stratification effects. Building on the knowledge that the highest efficiency of oscillatory propulsion consistently occurs within a narrow St interval in homogeneous fluids, we conduct new numerical simulations to examine the optimal Strouhal numbers for an oscillating foil in a density stratified fluid. This study seeks to provide new insights into the role of density stratification in optimising Strouhal numbers of oscillatory propulsion and offer novel information for flow patterns generated by oscillating bodies in stratified regimes.

2. Methodology

2.1. *Problem formulation and governing parameters*

We consider a two-dimensional NACA0012 aerofoil undergoing combined heaving $h(t)$ and pitching $\theta(t)$ motion in a uniform inflow with a constant velocity U_∞ (see figure 1*a*). The aerofoil rotates about a pivot point with a distance b from the leading edge. The foil's motion is described by

$$h(t) = h_0 \sin(2\pi f t), \quad \theta(t) = \theta_0 \sin(2\pi f t + \phi), \tag{2.1}$$

where f is the oscillation frequency, h_0 is the heave amplitude, θ_0 is the pitch amplitude, and ϕ is the phase difference between heave and pitch. As illustrated in figure 1(*b*), the instantaneous angle of attack $\alpha(t)$ is given by

$$\alpha(t) = \arctan\left(\frac{1}{U_\infty}\frac{\mathrm{d}h(t)}{\mathrm{d}t}\right) - \theta(t). \tag{2.2}$$

When the pitch leads the heave by $\phi = 90°$, the maximum angle of attack α_0 can be obtained by

$$\alpha_0 = \arctan\left(\frac{2\pi h_0 f}{U_\infty}\right) - \theta_0. \tag{2.3}$$

The choice of aerofoil geometry and inflow velocity in our simulations follows the set-ups of the experiments by Anderson *et al.* (1998) and Read *et al.* (2003), ensuring that the involved parameters are relevant to biological propulsion in nature.

For a foil that simultaneously heaves and pitches in density stratified fluids, three dimensionless parameters govern the problem: the chord-based Reynolds number Re, the amplitude-based Strouhal number St and the internal Froude number Fr:

$$Re = \frac{U_\infty c}{\nu}, \quad St = \frac{2h_0 f}{U_\infty}, \quad Fr = \frac{U_\infty}{ND}, \tag{2.4}$$

where ν is the kinematic viscosity, D is the maximum thickness of the foil and N is the Brunt–Väisälä frequency signifying the natural oscillation frequency of fluid particles in a stratified fluid. The above expression for St is based on the approximation that the characteristic width of the wake is equivalent to the lateral total excursion of the foil (Triantafyllou *et al.* 2000). We consider a linearly stratified fluid with a constant density gradient γ in the direction of gravitational acceleration $\boldsymbol{g}$. The background density profile is set as $\rho_b(y) = \rho_0 - \gamma y$ (see figure 1*a*), where ρ_0 is the reference fluid density and y is the vertical coordinate. The Brunt–Väisälä frequency is given by $N = (\gamma g/\rho_0)^{1/2}$.

https://doi.org/10.1017/jfm.2025.283 Published online by Cambridge University Press

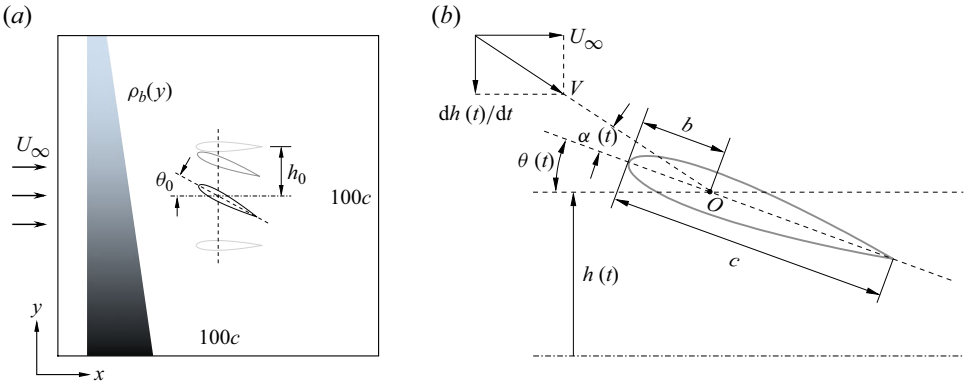


Figure 1. (*a*) Schematic of the computational domain with a size of $100c \times 100c$. The initial background density is set as a linear profile: $\rho_b(y) = \rho_0 - \gamma y$, with a constant density gradient γ along the y direction. Note that foil size is exaggerated for better visibility. (*b*) Illustration of the foil kinematics, where the foil performs combined heaving $h(t)$ and pitching $\theta(t)$ motion in a uniform inflow with a constant velocity U_∞, leading to an instantaneous angle of attack $\alpha(t)$.

We select the value of γ to ensure that the maximum density variation does not exceed 5 % of ρ_0, thereby satisfying the Boussinesq approximation for stratified fluids. When executing a fully prescribed motion, the oscillating foil is assumed to maintain a neutrally buoyant state. Therefore, the desired Fr can be easily achieved by adjusting g in our simulations.

The primary parameters in this study are selected as $h_0/c = 0.75$, $\phi = 90°$, $\alpha_0 = 15°$ and $b/c = 1/3$. These values are chosen based on previous studies indicating that such parameter settings tend to yield satisfactory propulsive performance for oscillating foils in homogeneous fluids (Anderson *et al.* 1998; Read *et al.* 2003). However, whether this combination of parameters represents an optimal choice for stratified fluids remains an open question. The frequency f is adjusted to achieve the desired St and the constant α_0 is attained by varying θ_0. The Reynolds number is fixed at $Re = 1000$ for all simulations. This relatively low-turbulence regime has been widely studied in the context of hydrodynamic performance and wake evolution of oscillating foils (Anderson *et al.* 1998; Godoy-Diana *et al.* 2008; Verma & Hemmati 2022), suggesting that Reynolds numbers of the order of $O(10^3)$ are sufficient to capture key features of oscillating-based propulsion. Moreover, Gazzola *et al.* (2014) performed a comprehensive analysis on biological measurements and found that the preferred Strouhal number of swimming animals stabilises once the Reynolds number, based on body length, exceeds a critical value. In our simulations, the chord-length Reynolds number corresponds to a body-length Reynolds number within a flow regime where the Reynolds number has minimal effect on the Strouhal number (Gazzola *et al.* 2014).

Our central focus is on the parameter space defined by St, characterising the foil kinematics, and Fr, characterising the stratification strength. The St and Fr are varied within the ranges of $0.1 \leqslant St \leqslant 0.6$, with an interval $\Delta St = 0.05$, and $1 \leqslant Fr \leqslant 10$, with an interval $\Delta Fr = 0.5$. This St range covers the majority of Strouhal numbers observed in natural swimmers and examined in the studies of oscillating foils. The Fr range considered here encompasses a spectrum of stratification strengths from strong to weak. Given typical N values in real stratified environments (Thorpe 2005), the internal Froude numbers for biological appendages or artificial foils with a length scale of $O(1\text{m})$ can fall within the considered Fr range when cruising at feasible speeds.

https://doi.org/10.1017/jfm.2025.283 Published online by Cambridge University Press

A combined heaving and pitching foil experiences instantaneous streamwise force $F_x(t)$, transverse force $F_y(t)$ and torque $Q(t)$ about the rotation axis. The time-averaged thrust production and input power over one oscillation cycle T are calculated by

$$\bar{F} = \frac{1}{T}\int_0^T F_x(t)\mathrm{d}t, \tag{2.5}$$

$$\bar{P} = \frac{1}{T}\left(\int_0^T F_y(t)\frac{\mathrm{d}h(t)}{\mathrm{d}t}\mathrm{d}t + \int_0^T Q(t)\frac{\mathrm{d}\theta(t)}{\mathrm{d}t}\mathrm{d}t\right). \tag{2.6}$$

The performance metrics of an oscillating foil are characterised by the time-averaged thrust coefficient C_T, power coefficient C_P and propulsive efficiency η:

$$C_T = \frac{\bar{F}}{0.5\rho_0 U_\infty^2 cs}, \quad C_P = \frac{\bar{P}}{0.5\rho_0 U_\infty^3 cs}, \quad \eta = \frac{\bar{F}U_\infty}{\bar{P}} = \frac{C_T}{C_P}, \tag{2.7}$$

where s denotes the foil span, taking as unit length in two-dimensional cases. Each simulation is run for eight oscillation cycles, with time-averaged results computed from the final cycle. Our findings indicate that the system reaches a periodic state by the fourth oscillation cycle. In this study, both instantaneous and time-averaged force metrics are normalised using the free stream velocity as the velocity scale and the aerofoil chord length as the length scale, following the conventions established in studies of oscillatory propulsion. This normalisation allows for direct comparison of the propulsive characteristics between the present stratified fluid results and relevant homogeneous observations in the literature. It is noteworthy that recent experiments and theories suggest more appropriate scales for hydrodynamic performance of oscillating foils (Smits 2019). One can refer to newly proposed scaling laws for more details (Floryan *et al.* 2017; Van Buren *et al.* 2019).

2.2. *Numerical methods*

The two-dimensional incompressible stratified flow around an oscillating foil is simulated using a finite-volume solver. The fluid motion is governed by the conservation equations of mass, momentum and density under the Boussinesq approximation, assuming that the density variations appear only in the buoyancy force term and are negligible compared with the reference density. The density ρ and pressure p fields are split into background and fluctuating components, expressed as $\rho = \rho_b + \rho'$ and $p = p_b + p'$. The background density ρ_b follows a linear profile, as previously specified. The background pressure p_b satisfies the hydrostatic balance $\nabla p_b = \rho_b \boldsymbol{g}$. The fluctuating quantities, ρ' and p', arise from the fluid motion. The governing equations are therefore given by

$$\nabla \cdot \boldsymbol{u} = 0, \tag{2.8}$$

$$\frac{\partial \boldsymbol{u}}{\partial t} + \boldsymbol{u}\cdot\nabla\boldsymbol{u} = -\frac{1}{\rho_0}\nabla p' + \nu\nabla^2\boldsymbol{u} + \frac{\rho'}{\rho_0}\boldsymbol{g}, \tag{2.9}$$

$$\frac{\partial \rho'}{\partial t} + \boldsymbol{u}\cdot\nabla\rho' + \boldsymbol{u}\cdot\nabla\rho_b = \frac{\nu}{Pr}\nabla^2(\rho_b + \rho'), \tag{2.10}$$

where $\boldsymbol{u}$ is the fluid velocity, t denotes time and Pr is the Prandtl number, representing the ratio of momentum to thermal diffusivity. Given that temperature variation is the primary factor influencing density changes in aquatic environments (Sutherland 2010), we set the Prandtl number to $Pr = 7$, a typical value for thermally stratified fluids. In our numerical simulations, the grid spacing near the foil surface is carefully designed to resolve both the momentum and density boundary layers for the Reynolds and Prandtl numbers considered.

https://doi.org/10.1017/jfm.2025.283 Published online by Cambridge University Press

According to Schlichting & Gersten (2016), the boundary-layer thicknesses for momentum and density can be estimated as $\delta_m \sim O(D/\sqrt{Re})$ and $\delta_d \sim O(D/\sqrt{RePr})$, respectively.

The configuration of the computational domain is illustrated in figure 1(*a*). We use an arbitrary Lagrangian–Eulerian formulation to solve the governing equations on a moving grid, which comprises two zones interconnected through a circular sliding interface. The inner circular zone, with a radius of $10c$, undergoes rigid rotation to account for the foil pitch, while grid deformation in the outer zone implements the foil heave. To prevent spurious reflection of internal waves, our numerical model employs a significantly large domain size ($100c \times 100c$) with considerable distances between the foil and boundaries.

The solver uses the first-order implicit Euler scheme to advance the equations in time. The spatial derivatives of convection and diffusion terms are discretised using second-order upwind and central-difference schemes, respectively. The pressure–velocity coupling is resolved using the pressure implicit with splitting of operators (PISO) algorithm. We set the boundary condition of the oscillating foil as a moving wall with no flux normal to the surface. A uniform constant velocity is imposed at the inlet boundary, while the outlet boundary employs a convective outflow condition. The pressure field is treated with a Dirichlet boundary condition at the top and a Neumann boundary condition at the other boundaries. A Neumann boundary condition is applied at all boundaries for the density field.

It is noteworthy that the momentum equation employed in our previous study (Wang *et al.* 2024) is

$$\frac{\partial \boldsymbol{u}}{\partial t} + \boldsymbol{u}\cdot\nabla\boldsymbol{u} = -\frac{1}{\rho_0}\nabla p'' + \nu\nabla^2\boldsymbol{u} - \frac{\boldsymbol{g}\cdot\boldsymbol{r}}{\rho_0}\nabla\rho, \tag{2.11}$$

where $\boldsymbol{r} = (x, y, z)$ is the position vector and p'' represents the flow-induced pressure. Both (2.11) and (2.9) are derived from the standard incompressible momentum equation based on the Boussinesq approximation. They are mathematically equivalent with the only difference in the form of the flow-induced pressure. From a computational standpoint, solving the density perturbation directly (the last term on the right-hand side of (2.9)) is found to double the computational time compared with solving the gradient of density perturbation (the last term on the right-hand side of (2.11)). That is why (2.11) was used in our previous study (Wang *et al.* 2024). By solving (2.11), we have $p = p'' + \rho\boldsymbol{g}\cdot\boldsymbol{r}$, where $\rho\boldsymbol{g}\cdot\boldsymbol{r}$ approximates the hydrostatic pressure component, as ρ' is insignificant compared with ρ_0. However, our recent computations indicate that despite $\rho' \ll \rho_0$, the approximation of $p_b = \rho\boldsymbol{g}\cdot\boldsymbol{r}$ leads to an overestimate in the thrust production of oscillating foils.

In the current study, we solve (2.9) to obtain the flow-induced pressure p'. This approach yields $p = p' + 0.5(\rho_0 + \rho_b)\boldsymbol{g}\cdot\boldsymbol{r}$, where the hydrostatic pressure component $p_b = 0.5(\rho_0 + \rho_b)\boldsymbol{g}\cdot\boldsymbol{r}$ is calculated through the hydrostatic balance $\nabla p_b = \rho_b\boldsymbol{g}$, along with the linear background density $\rho_b(y) = \rho_0 - \gamma y$. The hydrostatic pressure component can be rearranged as $p_b = -\rho_0 g y + 0.5 g\gamma y^2$, consistent with Ardekani & Stocker (2010). This update is believed to provide more accurate predictions for the hydrodynamic performance of an oscillating foil in stratified fluids. The correction of the hydrostatic pressure is the primary cause of the discrepancies between the results presented in this study and those reported in our previous work (Wang *et al.* 2024). Additionally, the Prandtl number was set to $Pr = 1$ in our previous simulations (Wang *et al.* 2024), which accounts for a discrepancy less than 10 %.

The numerical solver used in this study has been extensively validated and successfully applied to various problems involving stratified fluids (Deng & Kandel 2022; Kandel & Deng 2022; Wang *et al.* 2023*a*,*b*). In the Appendix, a sensitivity analysis is performed

https://doi.org/10.1017/jfm.2025.283 Published online by Cambridge University Press

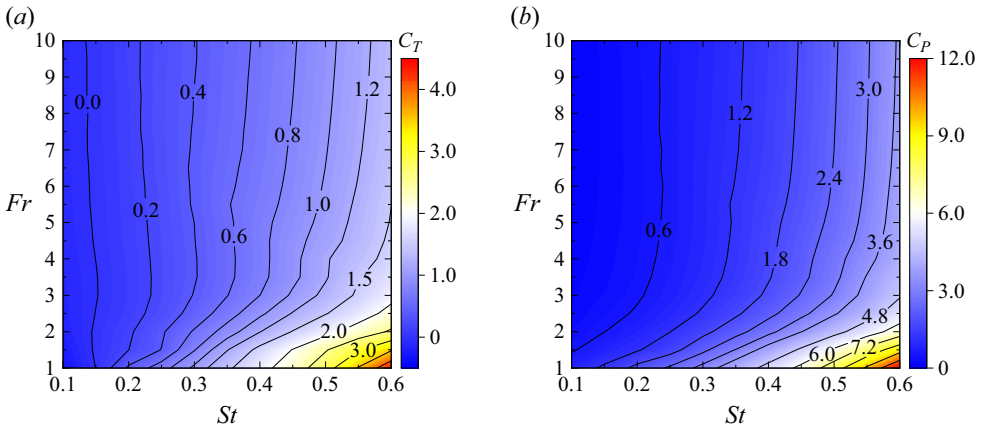


Figure 2. Contour plots of time-averaged (*a*) thrust coefficient C_T and (*b*) power coefficient C_P over one oscillation cycle for an oscillating foil in the (St, Fr) parameter space.

concerning grid resolution, time step and computational domain size for the most challenging case ($St = 0.6$, $Fr = 1$) within the parameter space considered here.

3. Parametric studies on propulsive performance

We carry out a parametric study by scanning the (St, Fr) parameter space, which covers the ranges of $0.1 \leqslant St \leqslant 0.6$ and $1 \leqslant Fr \leqslant 10$. Our focus is on identifying the optimal Strouhal numbers St_m for oscillatory propulsion in stratified fluids. We first present primary observations here and then elucidate underlying mechanisms driving these behaviours in the subsequent sections. We limit the discussion of the foil's optimal kinematic conditions to the Strouhal number alone. Given that the propulsive performance of an oscillating foil is influenced by a wide range of kinematic and geometric parameters, it is expected that altering the parameters held constant in our simulations could also yield high thrust production and efficiency in stratified fluids, similar to the effects achieved by tuning the Strouhal number. This may lead to the identification of other optimal conditions, which remains an open question for future research.

Figure 2 displays the contour plots for time-averaged thrust and power coefficients. The oscillating foil initially generates drag at very low St, which transitions to thrust as St increases. Both thrust and power under the stratification influence increase monotonically with St, aligning with the observations in homogeneous fluids. However, the rate of change of C_T and C_P with St depends on the Froude number. Significant variations in thrust and power are observed at low Fr, resulting in high-intensity regimes in the lower-right corner of the (St, Fr) plane. The monotonic variation of time-averaged metrics in figure 2 indicates that C_T and C_P can be scaled with a combination of St and Fr. Inspired by extensive efforts to scale oscillatory propulsion in homogeneous fluids (Quinn *et al.* 2014; Floryan *et al.* 2017; Van Buren *et al.* 2019) and the scaling laws derived by Zhang *et al.* (2019) for the drag on a settling body in stratified fluids, we propose a simplified scaling relation to characterise the numerical data presented in this study:

$$C_T = c_1 St^{\alpha_1} Fr^{\beta_1}, \quad C_P = c_2 St^{\alpha_2} Fr^{\beta_2}. \tag{3.1}$$

By minimising the squared residuals, the coefficients are determined as follows: $c_1 = 11.79$, $\alpha_1 = 2.09$, $\beta_1 = -0.56$ for C_T and $c_2 = 30.53$, $\alpha_2 = 2.01$, $\beta_2 = -0.62$ for C_P. Note that these coefficients are specific to the current dataset and should not be regarded as

https://doi.org/10.1017/jfm.2025.283 Published online by Cambridge University Press

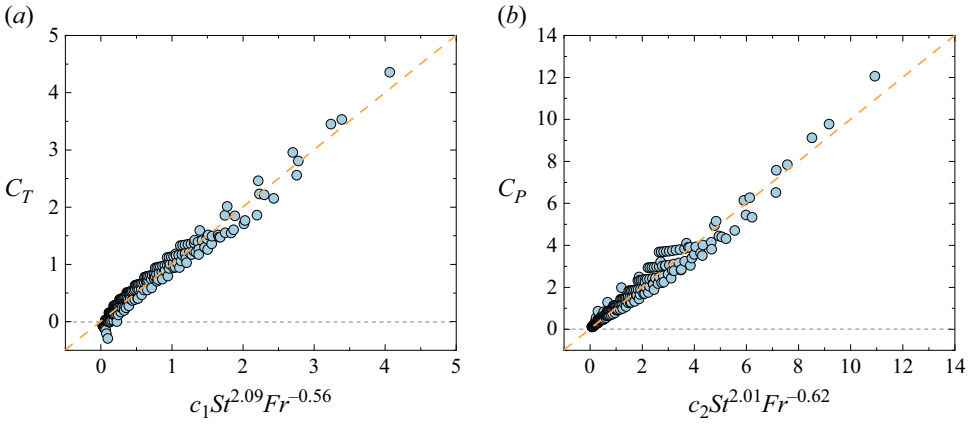


Figure 3. Time-averaged (a) thrust coefficient C_T and (b) power coefficient C_P over one oscillation cycle as functions of the presented scaling relations, where $c_1 = 11.79$ and $c_2 = 30.53$.

universal. Figure 3 plots all C_T and C_P data as a function of the proposed scaling relation. Overall, the collapse of the data is satisfactory for both thrust and power, suggesting that the principal parameters St and Fr considered in our simulations adequately capture the key flow physics of oscillating foils in a density stratified fluid. It is worth noting that the leading role of St^2 in the scaling of oscillatory propulsion in homogeneous fluids (Floryan *et al.* 2017; Van Buren *et al.* 2019) closely aligns with the St component in our proposed scaling relations.

In contrast, the propulsive efficiency η shows complex variations within the (St, Fr) parameter space, as depicted in figure 4(a). The efficiency is seen to increase rapidly with St at first and then decrease gently at higher St, indicating the existence of an optimal St for oscillating foils in stratified fluids. Notably, a multimodal pattern emerges, characterised by a first peak of $\eta = 0.47$ at ($St = 0.35$, $Fr = 5.5$) and a second peak of $\eta = 0.43$ at ($St = 0.45$, $Fr = 2.5$). This suggests that the optimal St of oscillatory propulsion in stratified fluids greatly depends on stratification strength.

The geometric and kinematic parameters considered here give rise to an optimal Strouhal number of $St_m = 0.35$ for homogeneous fluids, which falls exactly within the typical range of 0.20–0.40. Based on the observations in figure 4(a), we use $Fr = 5.0$ to divide the stratified regimes into weak stratifications ($Fr \geqslant 5$), where St_m of stratified fluids remains largely consistent with that of homogeneous fluids, and strong stratifications ($Fr < 5$), where St_m of stratified fluids differs significantly from its homogeneous counterpart. To identify St_m in the strong-stratification regime ($Fr < 5$), we perform a finer parametric sweep with an interval of $\Delta St = 0.01$. The optimal Strouhal numbers from our numerical simulations are summarised by black circles in figure 4(b). We observe that St_m in stratified fluids tends to increase as Fr decreases. In weakly stratified fluids ($Fr \geqslant 5$), the influence of density stratification on the optimal condition is minimal. However, as stratification intensifies ($Fr < 5$), St_m in stratified fluids begins to exceed the values of homogeneous cases. Notably, when $Fr < 3$, the optimal Strouhal numbers under stratification effects fall outside the typical range observed in homogeneous fluids.

Given that both the Strouhal number and the Froude number include a frequency component, we can intuitively relate the dependence of St_m on Fr to resonance behaviour. As indicated by (2.4), the oscillating frequency f in St characterises the foil kinematics, while the Brunt–Väisälä frequency N in Fr is an inherent property for stratified fluids. Assuming a resonance between these two frequencies such that $f/N \sim O(1)$, we can

https://doi.org/10.1017/jfm.2025.283 Published online by Cambridge University Press

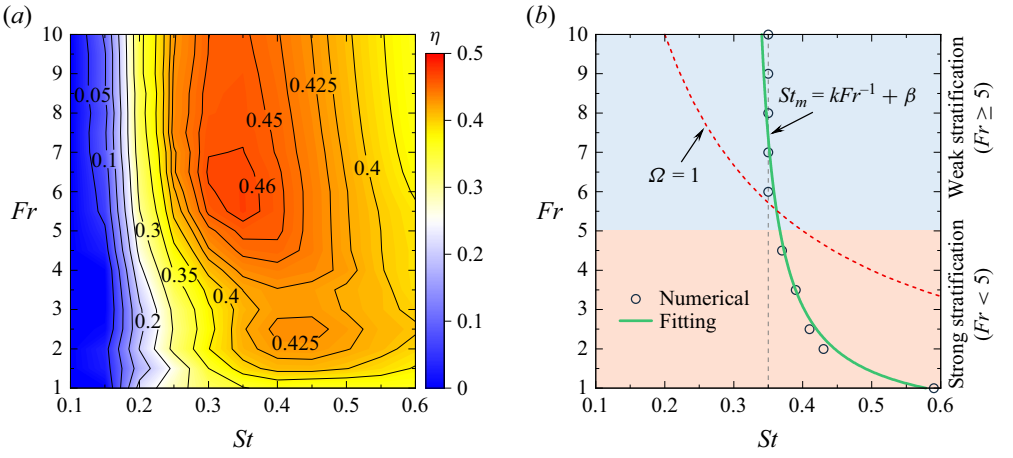


Figure 4. (*a*) Contour plots of propulsive efficiency η for an oscillating foil within the (St, Fr) parameter space. (*b*) Optimal Strouhal number St_m that produces the highest propulsive efficiency across the range of Froude numbers considered here. The black circles represent the results from numerical simulations and the green solid line indicates a fitting formula based on these numerical results. $Fr = 5.0$ is used to classify weak ($Fr \geqslant 5$) and strong ($Fr < 5$) stratifications. The grey dashed line marks the optimal Strouhal number in a homogeneous fluid ($St_m = 0.35$). The red dashed line indicates an alternative boundary with $\Omega = 1$ that separates the parameter space into lower-left strongly stratified regime ($\Omega < 1$) and upper-right weakly stratified regime ($\Omega > 1$).

infer that $St \sim Fr^{-1}$. Accordingly, we employ the following function to fit our numerical results:

$$St_m = kFr^{-1} + \beta, \tag{3.2}$$

where k and β are fitting coefficients. As shown by the green solid line in figure 4(*b*), the fitting function (3.2) with $k = 0.264$ and $\beta = 0.314$ accurately represents our numerical results. In particular, the coefficient β closely matches the optimal Strouhal number for the homogeneous case, which is reasonable because $Fr = \infty$ in (3.2) leads to $St_m = \beta$. The coefficient of k, which depends on the foil kinematics, can be determined through numerical analysis. By appropriately finalising the values of k and β, (3.2) can be used to predict the optimal operating conditions of oscillatory systems in stratified environments.

The good agreement between the current simulations and predictions by (3.2) confirms an inherent coupling between the oscillating frequency and the Brunt–Väisälä frequency. The optimum efficiency seems to occur when f is comparable to N, triggering resonance between the foil and fluid oscillations. To achieve this resonance, the oscillating frequency f needs to be sufficiently large to match the relatively high Brunt–Väisälä frequency N at strong stratifications. This explains the higher St_m observed in strongly stratified fluids. It is worth pointing out that this resonance mechanism aligns with observations by Triantafyllou *et al.* (1991, 1993), who noted that maximum efficiency occurs within a narrow range of Strouhal numbers where the foil's oscillatory frequency matches the frequency of maximum spatial amplification of flow disturbances. Additionally, Tkacheva (1995, 1998) conducted a theoretical analysis of an infinitely thin plate moving in a stratified fluid, supplemented by a series of numerical calculations. Under the assumption of inviscid flow, they found that the hydrodynamic characteristics of a harmonically vibrating plate are highly dependent on the relationship between the Strouhal number and the inverse Froude number.

https://doi.org/10.1017/jfm.2025.283 Published online by Cambridge University Press

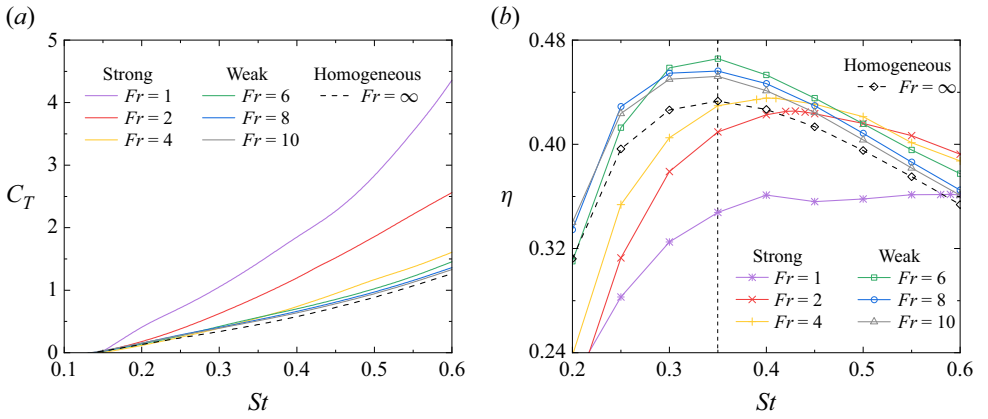


Figure 5. Comparison of (*a*) time-averaged thrust coefficient and (*b*) propulsive efficiency between stratified and homogeneous cases as a function of Strouhal number. Note that $Fr = \infty$ corresponds to the homogeneous fluid, where the optimal Strouhal number is $St_m = 0.35$.

It should be noted that in this study, we use a Froude number threshold of $Fr = 5.0$ to distinguish between weakly and strongly stratified regimes. This choice is based on the observation that the optimal Strouhal numbers in stratified fluids converge to their homogeneous counterparts when Fr exceeds 5.0. For oscillation in a uniformly stratified fluid, the dimensionless frequency ratio, defined as $\Omega = \omega_f/\omega_0$, where ω_f and ω_0 represent the oscillatory frequency and the Brunt–Väisälä frequency (both in radians per second), is a key parameter that governs the dynamical behaviours. Since Ω characterises the relative contributions of inertial effects due to oscillation and buoyancy effects of density stratification, the boundary at $\Omega = 1$ serves as an alternative criterion to separate weak and strong stratifications. By combining $\Omega = 1$ with the kinematics of the oscillating foil, we obtain the boundary $Fr = 2/St$, which is represented by the red dashed line in figure 4(*b*).

Further comparison of propulsive performance between stratified fluids and homogeneous environments is shown in figure 5. After correcting the numerical implementation as described in § 2.2, the time-averaged thrust coefficient and propulsive efficiency presented here are lower than those reported in our previous study (Wang *et al.* 2024). However, the qualitative enhancement of both thrust production and efficiency due to stratification effects remains consistent with our previous findings. Figure 5(*a*) shows that the oscillating foil generates a higher thrust across the entire Strouhal number range in stratified fluids compared with the homogeneous case. In contrast, the improvement in efficiency is found to be more sensitive to the strength of stratification, as depicted in figure 5(*b*). The oscillating foil tends to achieve a higher efficiency regardless of St than the homogeneous counterpart at weak stratifications. The notable discrepancy in efficiency can be observed even at a Froude number as high as $Fr = 10$, highlighting the significant role of stratification effects in oscillatory propulsion. Our numerical test indicates that such a discrepancy exists until Fr approaches $O(100)$. In strongly stratified fluids, the stratification effects only contribute to efficiency performance when the Strouhal number exceeds a certain value. Importantly, the oscillating foil under all considered stratifications produces a more efficient propulsion compared with the homogeneous counterpart at $St = 0.6$. Considering that the thrust production at $(St = 0.6, Fr = 1.0)$ is 3.44 times higher than that in the homogeneous case, the oscillating foils with high Strouhal numbers can gain substantial propulsive benefits in strongly stratified fluids.

https://doi.org/10.1017/jfm.2025.283 Published online by Cambridge University Press

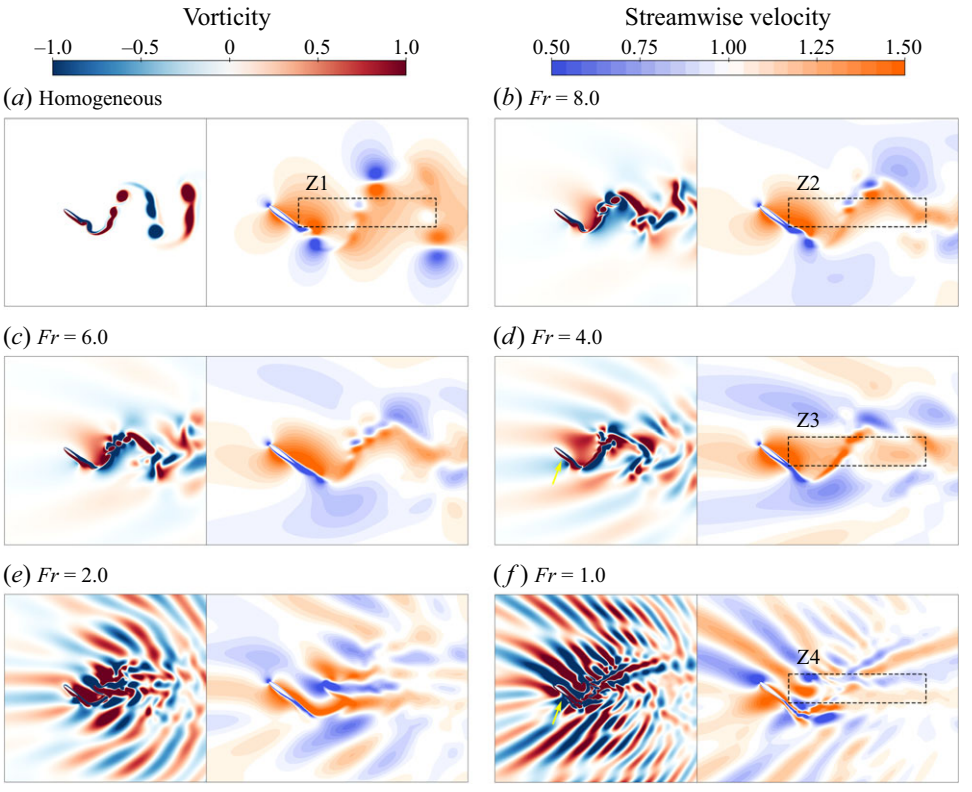


Figure 6. Instantaneous contours of vorticity and streamwise velocity at $St = 0.40$ for (a) homogeneous fluids and (b–f) stratified fluids with different Fr. In each plot, the left column shows the vorticity field normalised by U_∞/c and the right column exhibits the streamwise velocity field normalised by U_∞. The yellow arrows indicate the distinction in flow structures near the foil surface. The dashed squares highlight the difference in streamwise velocity jets around the centreline.

Figure 5(b) shows that maximum efficiency initially increases and then decreases as Fr decreases. This trend is attributed to the growing influence of induced internal waves on the flow structures around the oscillating foil. Figure 6 presents the instantaneous vorticity fields (left column of each panel) at $St = 0.40$ for various stratifications. At $Fr = 1.0$, the internal wave motion disrupts the boundary layer, causing significant flow detachment, as seen in figure 6(f). In contrast, the flow remains attached at lower stratification strengths (figure 6d). Flow separation is a known cause for the performance decline in oscillatory propulsion (Tuncer & Kaya 2005; Young & Lai 2007).

Moreover, it can be observed that the propulsive behaviour at $Fr = 1.0$ differs substantially from other cases, indicating a transition in flow physics as stratification strength increases. Figure 6 (right column of each panel) shows the instantaneous streamwise velocity fields. In weakly stratified fluids, velocity jets align with the centreline and cover a large area, consistent with the observations in homogeneous fluids (Z1 and Z2 in figure 6a,b). As Fr decreases, the induced jets tend to intensify in magnitude but narrow in vertical range (Z3 in figure 6d). At even lower Fr, the jets are seen to fragment and deviate from the centreline (Z4 in figure 6f). This jet shift from stable (Z2) to unstable (Z4) configurations with increasing stratification is similar to the findings of Akiyama *et al.* (2019). Especially, the stratification effects start to dominate the flow evolution at extremely strong stratification, leading to distinct behaviour at $Fr = 1.0$.

https://doi.org/10.1017/jfm.2025.283 Published online by Cambridge University Press

Figure 5(*b*) also provides a detailed comparison of the optimal Strouhal numbers between stratified and homogeneous fluids. It is evident that the optimal condition for weak stratifications aligns with the homogeneous case. However, in strongly stratified fluids, the peak efficiency occurs at Strouhal numbers outside the typical range of $0.20 < St < 0.40$ in a homogeneous fluid. At the strongest stratification ($Fr = 1$), the efficiency first increases sharply with the Strouhal number, and then decreases when St continues to rise. Notably, as St is further increased, the efficiency at $Fr = 1$ experiences a second rise, peaking at $St = 0.59$. This value is significantly higher than those observed in homogeneous fluids. Another important observation from figure 5(*b*) is that the decrease in efficiency when $St > St_m$ becomes less sensitive to the Strouhal number as stratification strength increases. This reduced sensitivity of efficiency performance to foil kinematics at relatively strong stratifications was also noted in our previous study (Wang *et al.* 2024), which examined different α_0 at a constant St.

Observation of high St_m at strong stratifications has several important implications. First, the well-established theories with respect to the performance optimisation of oscillatory propulsion in a homogeneous scenario (Triantafyllou *et al.* 2000; Tuncer & Kaya 2005; Izraelevitz & Triantafyllou 2014) may not be applicable to stratified fluids. This implies that man-made oscillatory propulsors should consider new parameter combinations and strategies to maximise efficiency in stratified environments. Next, oscillating foil propulsors in homogeneous fluids generally face a trade-off between thrust production and efficiency performance, where the optimal motion for efficiency tends to produce low thrust, and increasing thrust results in reduced efficiency (Smits 2019). Given that the efficiency in stratified fluids peaks at considerably large Strouhal numbers, the oscillating foils operating under stratification effects can achieve a sufficiently high thrust at optimal conditions. It has been observed that many aquatic species have preferred Strouhal numbers that deviate from universal principles (Eloy 2012; Gazzola *et al.* 2014), with most species entering a higher-St regime. This is consistent with our findings that the stratification effects increase the optimal Strouhal numbers of oscillating-based propulsion, suggesting that density stratification could be a probable cause for elevated Strouhal numbers observed in some organisms. Moreover, one significant insight from the optimal Strouhal numbers is that we can predict cruising speeds of animals using a simple rule of thumb, $U_c = 2h_0 f/St_m$. This is based on the assumption that natural selection optimises motion to match the optimal St values for maximum efficiency (Taylor *et al.* 2003). Our findings indicate that stratification effects need to be taken into consideration when applying such scaling rules to study animal locomotion.

4. Physical mechanisms for optimal Strouhal numbers

This section presents the physical interpretations behind the observed phenomena. We begin by taking a close look at the hydrodynamic aspects to gain fundamental insights, followed by an analysis of the flow field characteristics to uncover the underlying mechanisms. In this discussion, we mainly focus on $Fr = 2.0$ and $Fr = 6.0$ which are selected as representative cases for strong and weak stratifications, respectively.

4.1. *Hydrodynamic implications*

For an oscillating foil in a homogeneous fluid, the decrease in propulsive efficiency at high Strouhal numbers is typically due to either the slower nonlinear increase in thrust production compared with power expenditure, as suggested by scaling relations (Floryan *et al.* 2017; Van Buren *et al.* 2019), or a sudden drop of thrust caused by unsteady behaviours, such as severe flow separation around the foil surface (Isogai *et al.* 1999;

https://doi.org/10.1017/jfm.2025.283 Published online by Cambridge University Press

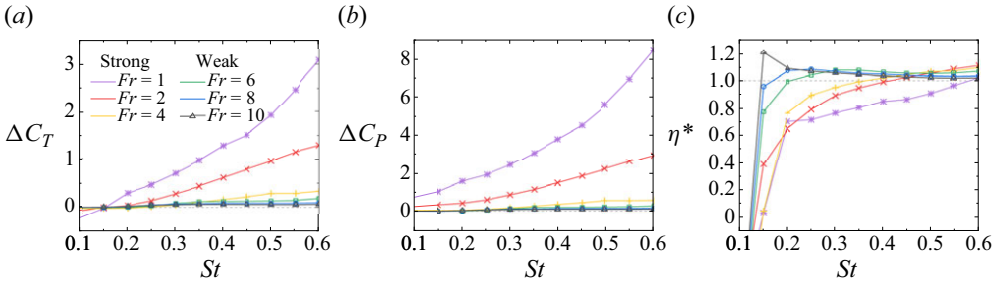


Figure 7. Stratification effects on the variation of (*a*) thrust production, (*b*) power expenditure and (*c*) efficiency ratio as a function of Strouhal number. Stratification-induced changes in thrust ΔC_T and power ΔC_P are calculated as $\Delta C_T = C_{Ts} - C_{Th}$ and $\Delta C_P = C_{Ps} - C_{Ph}$, respectively. The efficiency ratio η^* is defined as $\eta^* = \eta_s/\eta_h$. Here, subscripts s and h denote stratified and homogeneous conditions, respectively.

Young & Lai 2007). In either case, the efficiency begins to decline when the generated thrust cannot match the input power, suggesting that a continuous and robust increase in thrust with increasing Strouhal number plays a crucial role in shifting the optimum efficiency towards higher St.

To isolate the effects of stratification, we define the stratification-induced thrust production ΔC_T and power expenditure ΔC_P as the differences between the stratified and homogeneous results, i.e. $\Delta C_T = C_{Ts} - C_{Th}$ and $\Delta C_P = C_{Ps} - C_{Ph}$. Additionally, we define an efficiency ratio $\eta^* = \eta_s/\eta_h$ to indicate the relative efficiency of the stratified fluid compared with the homogeneous one. The cases where $\eta^* > 1$ indicate a higher efficiency in stratified fluids than the homogeneous counterpart.

Figure 7 illustrates the variations of ΔC_T, ΔC_P and η^* as a function of Strouhal number. As seen in figure 7(*a*), ΔC_T remains nearly constant for $Fr > 5$, whereas it exhibits an evident increase with St when $Fr < 5$. The invariable and low ΔC_T at $Fr > 5$ suggests that the stratification has an insignificant influence in weakly stratified fluids, resulting in optimal Strouhal numbers similar to those in homogeneous fluids. For strongly stratified regimes, ΔC_T at $Fr = 4$ first increases linearly with the Strouhal number and then stabilises when $St \geqslant 0.5$, while a linear rise in ΔC_T across the entire St range is observed for $Fr = 2$. Moreover, ΔC_T at $Fr = 1$ shows a much more rapid nonlinear increase compared with other cases. The optimal St values for $Fr = 1$, 2 and 4 are respectively 0.59, 0.43 and 0.40, indicating that higher optimal Strouhal numbers at stronger stratifications are due to the increasingly rapid rise in stratification-induced thrust production.

The variation of ΔC_P with the Strouhal number follows a similar trend as ΔC_T, as shown in figure 7(*b*). It is noted that an oscillating foil can achieve a high efficiency in stratified fluids as long as the stratification-induced thrust continues to rise significantly with St, despite the accompanying increase in power expenditure. Consequently, the efficiency ratio η^* changes differently with the Strouhal number across various stratified regimes (see figure 7*c*). With continuous increase in St crossing the optimal value, η^* at $Fr > 5$ slightly decreases and eventually converges to one, aligning weakly stratified fluids with homogeneous conditions. In contrast, η^* at $Fr < 5$ rises consistently and tends to deviate from one as St increases, highlighting that efficiency of strongly stratified fluids greatly outperforms the homogeneous counterpart at large Strouhal numbers.

We then turn to the instantaneous force characteristics which determine above distinct features of cycle-averaged metrics. For comparison, figure 8 displays the time-varying thrust and lift coefficients in a homogeneous fluid. As shown in figure 8(*a*), C_t peaks once

https://doi.org/10.1017/jfm.2025.283 Published online by Cambridge University Press

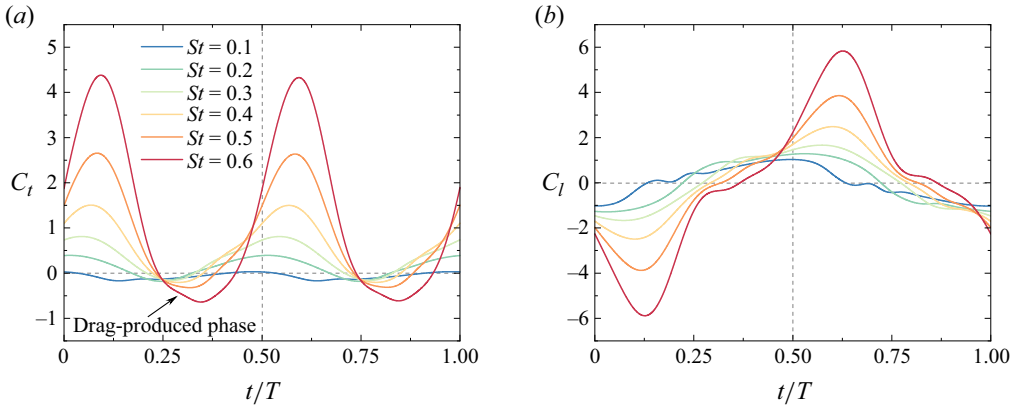


Figure 8. Time series of the instantaneous (*a*) thrust coefficient and (*b*) lift coefficient at various Strouhal numbers for $Fr = \infty$ (homogeneous fluid). The phase during which negative thrust is produced, indicated by $C_t < 0$, is defined as drag-produced phase.

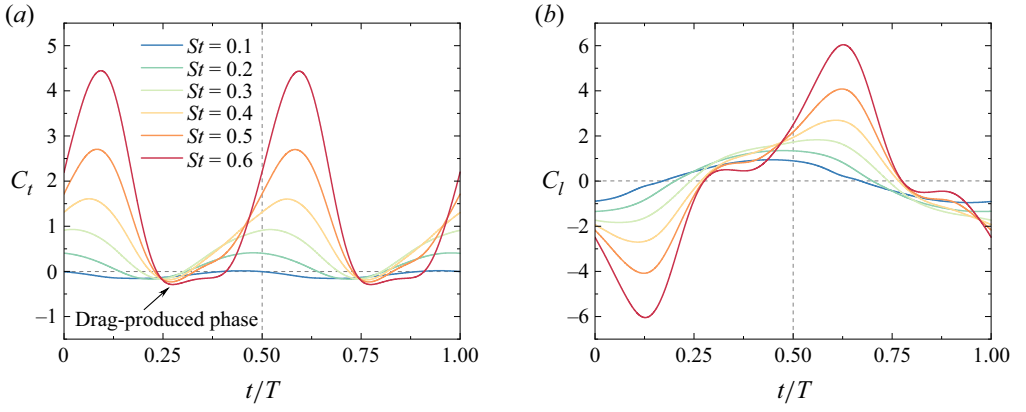


Figure 9. Time series of the instantaneous (*a*) thrust coefficient and (*b*) lift coefficient at various Strouhal numbers for $Fr = 6.0$ (weakly stratified fluid).

per half-oscillation cycle, during which a drag force rather than thrust is generated for a portion of the cycle, marked as drag-produced phase. From figure 8(*b*), we see that two opposing maxima appear in the time histories of C_l during each oscillation cycle. The peaks in both C_t and C_l increase with the Strouhal number. Notably, the drag-produced phase also becomes more significant in duration and magnitude at increasing Strouhal number (figure 8*a*), giving rise to a relatively larger proportion of drag force in total cycle-averaged streamwise force. As such, the expansion of drag-produced phase at a higher Strouhal number tends to retard the increase in C_T with St.

Figures 9 and 10 show the time evolution of instantaneous force coefficients at $Fr = 6.0$ (weak stratification) and $Fr = 2.0$ (strong stratification), respectively. The results show a clear difference in both the thrust and lift between homogeneous (figure 8) and stratified fluids (figures 9 and 10). Notably, the force characteristics at $Fr = 6.0$ differ significantly from those at $Fr = \infty$, indicating that even weak stratification influences the hydrodynamic performance of oscillating foils. This aligns with the cycle-averaged results in figure 5. However, weakly stratified and homogeneous cases exhibit similar Strouhal number dependence, with comparable increases in both maximum C_t and drag production

https://doi.org/10.1017/jfm.2025.283 Published online by Cambridge University Press

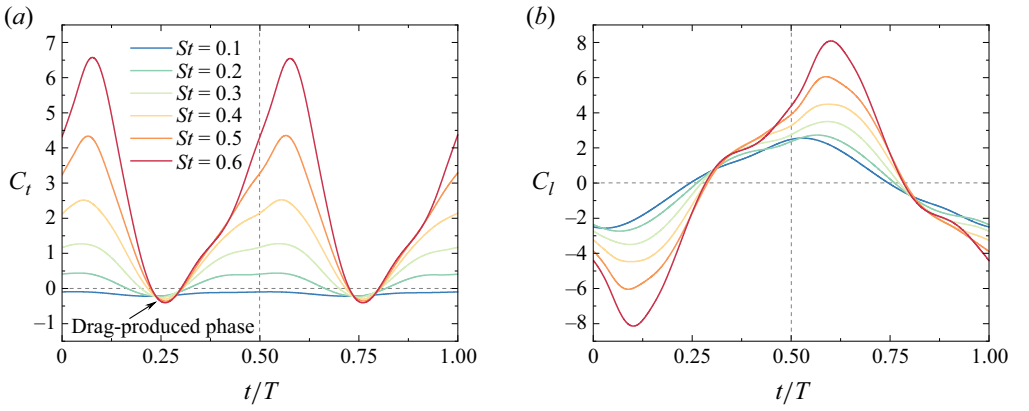


Figure 10. Time series of the instantaneous (*a*) thrust coefficient and (*b*) lift coefficient at various Strouhal numbers for $Fr = 2.0$ (strongly stratified fluid).

as St increases. Thus, the range of optimal St at weak stratifications matches that of homogeneous fluids (figure 4*b*). In contrast, the force characteristics at $Fr = 2.0$ show a distinct Strouhal number dependence, particularly for thrust, as seen in figure 10. First, the increase in maximum C_t with St is more pronounced at strong stratifications. For example, the peak C_t increases from 0.41 at $St = 0.2$ to 4.44 at $St = 0.6$ for the stratification level of $Fr = 6.0$, while it rises from 0.44 to 6.55 at the same Strouhal numbers for $Fr = 2.0$. Second, in strongly stratified fluids, the drag-produced phase shows much lower sensitivity to the Strouhal number, in contrast to the noticeable increase in drag production with St observed in weakly stratified fluids. As a result, the cycle-averaged thrust production in strongly stratified fluids does not suffer from drag-induced deterioration at high Strouhal numbers. These two features of C_t fundamentally contribute to the continuous and robust rise in stratification-induced thrust production at increasing St. Especially, the comparison of instantaneous forces between weak and strong stratifications further confirms that thrust production, rather than power expenditure, primarily governs the optimal Strouhal numbers in stratified fluids.

4.2. *Flow field analysis*

To better understand the force behaviours observed, we analyse the flow field features at three key instants during one oscillation cycle. The first instant, t_0, corresponds to the peak of the instantaneous thrust coefficient C_t, which occurs during the first half of the oscillation cycle (refer to figures 8, 9 and 10). The second and third instants are selected as $t_1 = 0.25T$ and $t_2 = 0.375T$, respectively, covering a drag-produced phase in homogeneous and weakly stratified fluids (refer to figures 8 and 9). Figures 11–13 present the influence of Strouhal number on the instantaneous pressure field p' in different flow regimes. In general, we can observe an evident difference in global pressure distribution between homogeneous and stratified cases. Specifically, compared with the homogeneous fluid, the pressure field in the stratified regimes tends to cover a larger region, due to the presence of internal waves. However, for the local pressure distribution near the oscillating foil, the weak stratification shows a similar Strouhal number dependence with the homogeneous counterpart, notably differing from the strongly stratified case.

The instant $t = t_0$ occurs in the first quarter of the oscillation cycle, when the foil performs upstroke motion. At this moment, a positive pressure region is formed on the upper surface of the foil, while the lower foil surface is surrounded by a negative pressure

https://doi.org/10.1017/jfm.2025.283 Published online by Cambridge University Press

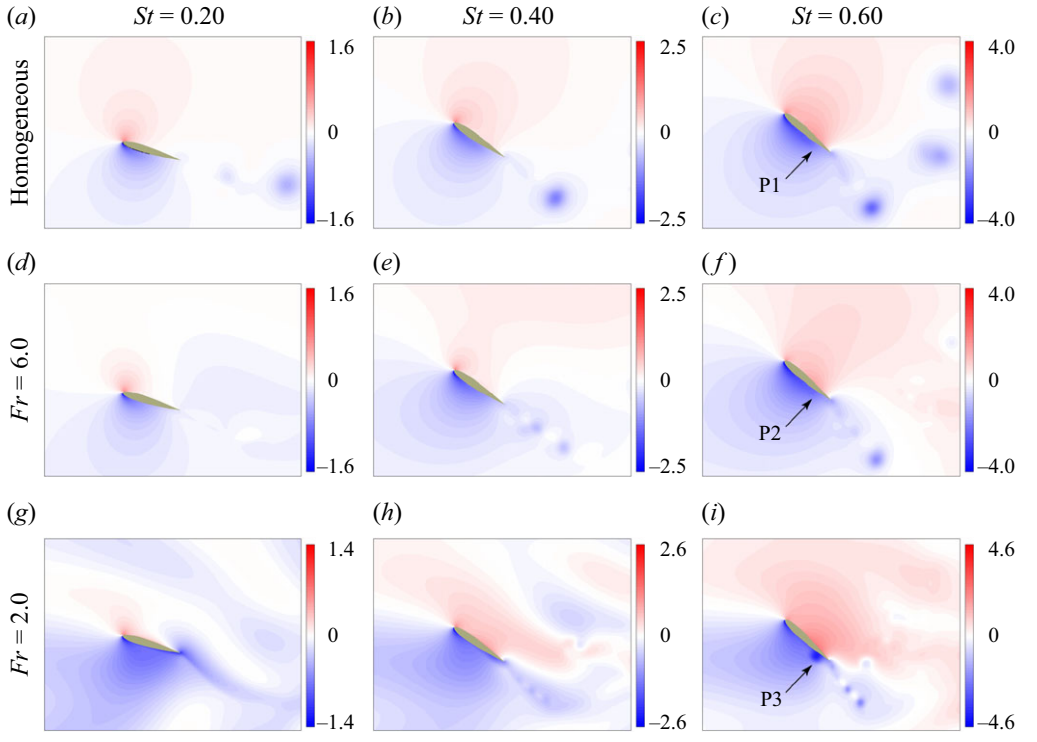


Figure 11. Influence of Strouhal number on instantaneous pressure field p', normalised by $\rho_0 U_\infty^2$, at the instant t_0 (corresponding to the first peak in C_t): $(a–c)$ for $Fr = \infty$; $(d–f)$ for $Fr = 6.0$; and $(g–i)$ for $Fr = 2.0$. The highlighted regions, labelled by P, indicate the distinction in pressure distribution between different flow regimes.

region, as shown in figure 11. These pressure distributions contribute to the streamwise component of force production, resulting in the maximum thrust coefficient. In both homogeneous and stratified fluids, the pressure regions near the foil are enhanced as the Strouhal number increases. However, when the Strouhal number becomes extremely high, an intense negative pressure aggregation forms below the trailing edge of the oscillating foil under strong stratifications (indicated by P3 in figure 11*i*). This pressure aggregation, which is absent in homogeneous and weakly stratified fluids (see P1 and P2 in figure 11*c*,*f*), contributes to the streamwise pressure difference, thereby improving thrust generation. Consequently, the rise in peak C_t with increasing St is more pronounced at $Fr = 2.0$ compared with $Fr = \infty$ and $Fr = 6.0$ (see figures 8*a*, 9*a* and 10*a*).

At $t = t_1$, the pressure distribution around the lower surface of the oscillating foil at $Fr = \infty$ is seen to evolve into an increasingly significant negative pressure region as the Strouhal number becomes higher (see A1, B1 and C1 in figure 12*a–c*). This behaviour results in an increase in drag force since the horizontal pressure difference surrounding the foil is directed downstream. Notably, the change in near-foil pressure distribution with the Strouhal number at $Fr = 6.0$ aligns with the homogeneous case, characterised by the growth of negative pressure aggregation around the lower foil surface, as shown by A2, B2 and C2 in figures 12(*d*)–12(*f*). In contrast, this variation in pressure distribution is less pronounced at $Fr = 2.0$ (see A3, B3 and C3 in figure 12*g–i*). Additionally, the strong stratification induces the distinct positive pressure aggregation above the trailing edge of the foil, which becomes more prominent as the Strouhal number increases. At a

https://doi.org/10.1017/jfm.2025.283 Published online by Cambridge University Press

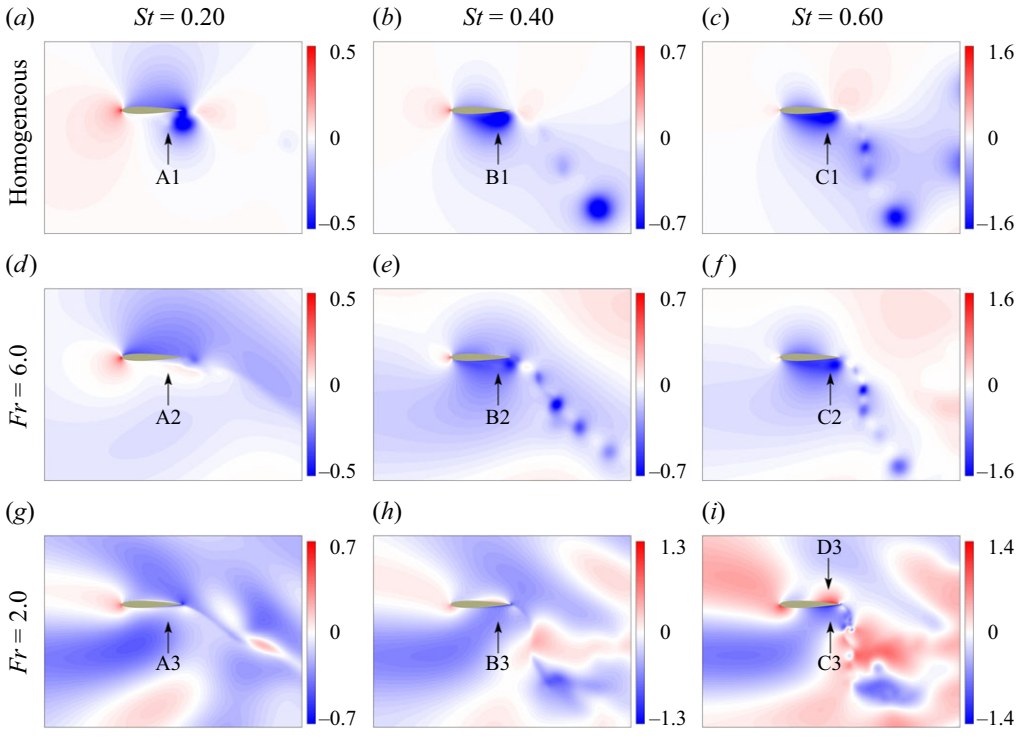


Figure 12. Influence of Strouhal number on the instantaneous pressure field p', normalised by $\rho_0 U_\infty^2$, at the instant t_1 ($t_1 = 0.25T$): (a–c) for $Fr = \infty$; (d–f) for $Fr = 6.0$; and (g–i) for $Fr = 2.0$. The highlighted regions, labelled by A, B, C and D, indicate the distinction in pressure distribution between different flow regimes.

high Strouhal number, this positive pressure aggregation (D3 in figure 12i) can partly compensate for the generated drag. As a result, the drag production at t_1 remains nearly constant in strongly stratified fluids (see figure 10a), while the negative C_t tends to increase with the Strouhal number in homogeneous and weakly stratified fluids, as shown in figures 8(a) and 9(a).

At $t = t_2$, the pressure distribution around the lower foil surface is dominated by a positive pressure region at $St = 0.20$, as shown in figures 13(a), 13(d) and 13(g). In homogeneous and weakly stratified fluids, this positive pressure aggregation tends to shrink with the increase in Strouhal number and is eventually replaced by a negative pressure region at $St = 0.60$ (see M1 and M2 in figure 13c,f). Moreover, when the Strouhal number increases to a specific level, a separate negative pressure aggregation forms behind the rear of the oscillating foil at $Fr = \infty$ (N1 in figure 13c) and $Fr = 6.0$ (N2 in figure 13f), contributing to drag production by directing the pressure difference in the direction opposite to swimming. Consequently, in homogeneous and weakly stratified fluids, the lower Strouhal numbers result in thrust production at $t = t_2$, which transitions to drag production at higher Strouhal numbers (see figures 8a and 9a). In strongly stratified fluids, however, the negative pressure region on the lower surface of the foil is less significant (see M3 in figure 13i) and the pressure distribution behind the trailing edge of the foil features a positive pressure aggregation (refer to N3 in figure 13i). This gives rise to the fact that the oscillating foil consistently produces a thrust force at $t = t_2$ as long as $St \geqslant 0.20$ (see figure 10a).

https://doi.org/10.1017/jfm.2025.283 Published online by Cambridge University Press

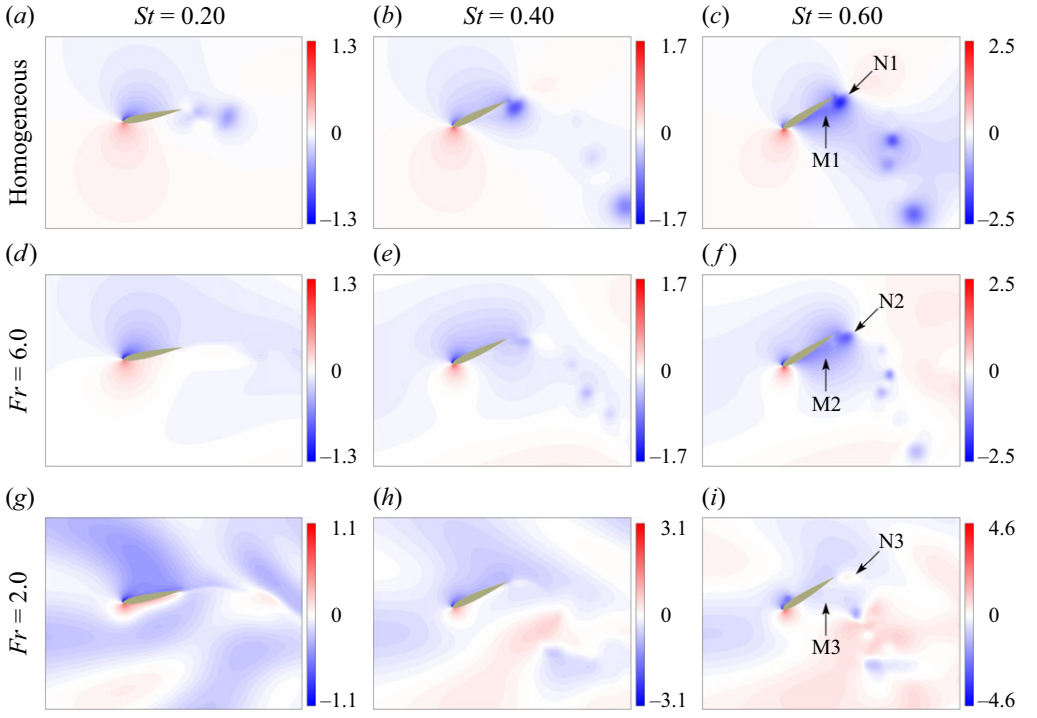


Figure 13. Influence of Strouhal number on the instantaneous pressure field p', normalised by $\rho_0 U_\infty^2$, at the instant t_2 ($t_2 = 0.375T$): (a–c) for $Fr = \infty$; (d–f) for $Fr = 6.0$; and (g–i) for $Fr = 2.0$. The highlighted regions, labelled by M and N, indicate the distinction in pressure distribution between different flow regimes.

In a density stratified fluid medium, the motion of objects can cause deflection of the isopycnals, leading to a violation of density conservation. This results in a volume of fluid being dragged to a position where its density differs from that of the surrounding fluid. Due to the buoyancy forces, this entrained fluid tends to move vertically, impacting the pressure distribution around the object. Fluid entrainment is considered a key mechanism responsible for the drag enhancement of settling bodies in a stratified fluid (Torres *et al.* 2000; Yick *et al.* 2009; Hanazaki *et al.* 2015; Zhang *et al.* 2019). In these studies, the vertical movement of a sphere results in the dragging of fluid with bilateral symmetry, which does not influence the horizontal component of force generation. However, for an oscillating foil with horizontally asymmetrical geometry and motion, the volume of dragged fluid near the leading edge is not equivalent to that around the trailing edge, consequently exerting an influence on the streamwise force production. We thus conjecture that asymmetric fluid entrainment by foil oscillation plays a crucial role in specific pressure distributions and resulting force behaviours observed in this study.

We compare the characteristics of pressure distribution and density perturbation at $St = 0.60$ in figure 14. The instantaneous pressure field is found to closely correlate with the instantaneous density field, suggesting that the density disturbance resulting from the dragging of fluids has a pivotal effect on the hydrodynamic performance of an oscillating foil. As illustrated by dashed squares in figure 14(b), an oscillating foil performing upstroke motion in a strongly stratified fluid pulls a volume of heavy fluid to a new vertical position, where the density is larger than that of the neighbouring fluid. The entrained fluid, in the form of an eddy structure, is forced to move downward due to buoyancy effects, inducing a negative pressure aggregation below the foil's trailing edge. At $t = t_1$, the negative pressure

https://doi.org/10.1017/jfm.2025.283 Published online by Cambridge University Press

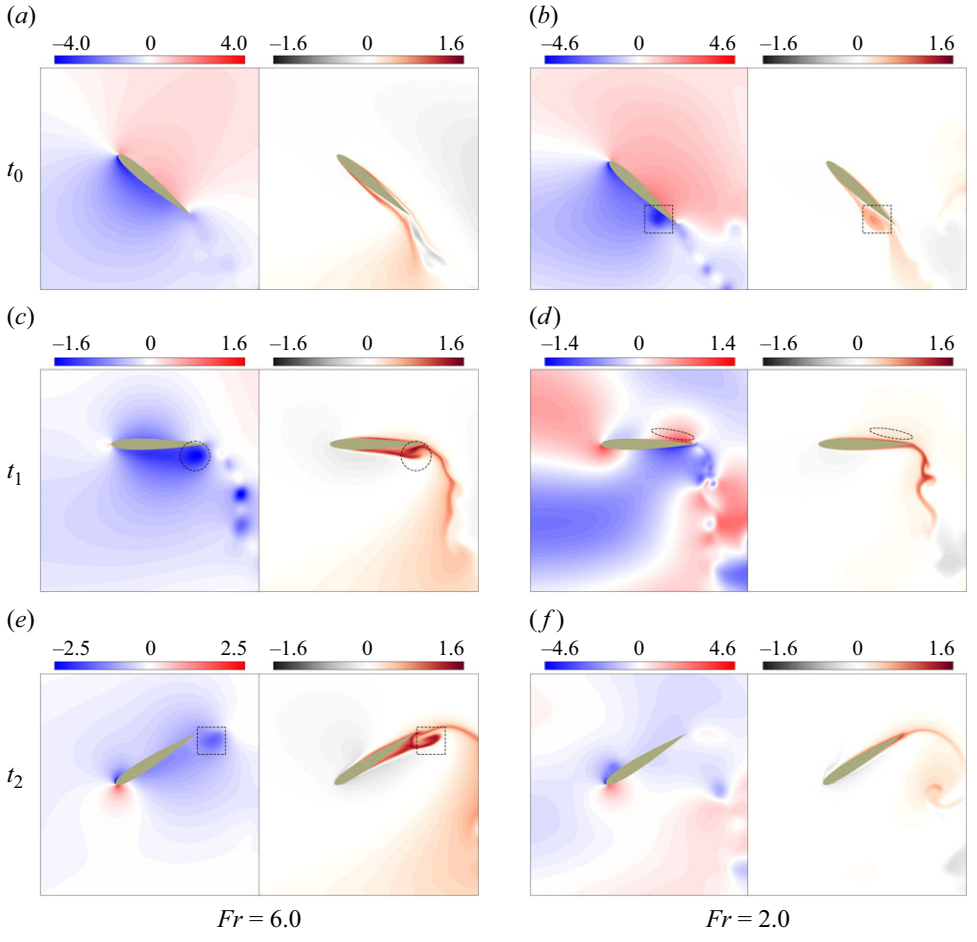


Figure 14. Comparison between instantaneous pressure field p' and density field ρ' for $St = 0.60$ at the instants of (*a*,*b*) $t = t_0$, (*c*,*d*) $t = t_1$ and (*e*,*f*) $t = t_2$. (*a*), (*c*) and (*e*) show results for weak stratification ($Fr = 6.0$), and (*b*), (*d*) and (*f*) for strong stratification ($Fr = 2.0$). The density ρ' is normalised by $\rho_0 cN^2/g$. The dashed squares, circles and ellipses highlight regions showing a close relationship between pressure distribution and density perturbation.

distribution around the lower rear of the oscillating foil in a weakly stratified fluid is clearly triggered by the density curling at the same area, as indicated by the dashed circles in figure 14(*c*). Conversely, the upper rear of the oscillating foil at $Fr = 2.0$ encounters an impact from the dragged heavy fluid, leading to a positive pressure distribution around this region, as shown by the dashed ellipses in figure 14(*d*). It is evident from the dashed squares in figure 14(*e*) that the prominent density destabilisation behind the foil's trailing edge at weak stratifications gives rise to a negative pressure aggregation in the downstream position. Such crucial impacts of fluid entrainment on pressure distribution and thus hydrodynamic forces have also been confirmed by studies on the free motion of bodies in density stratified fluids (Lam *et al.* 2019; Christin *et al.* 2021).

The dynamics of density perturbation are primarily determined by the relative magnitudes of inertial and buoyancy effects, characterised by the Froude number. Figure 15 exhibits the evolution of the density field over the first half of an oscillation cycle at $St = 0.60$. In weakly stratified fluids ($Fr = 6.0$), where inertial effects dominate,

https://doi.org/10.1017/jfm.2025.283 Published online by Cambridge University Press

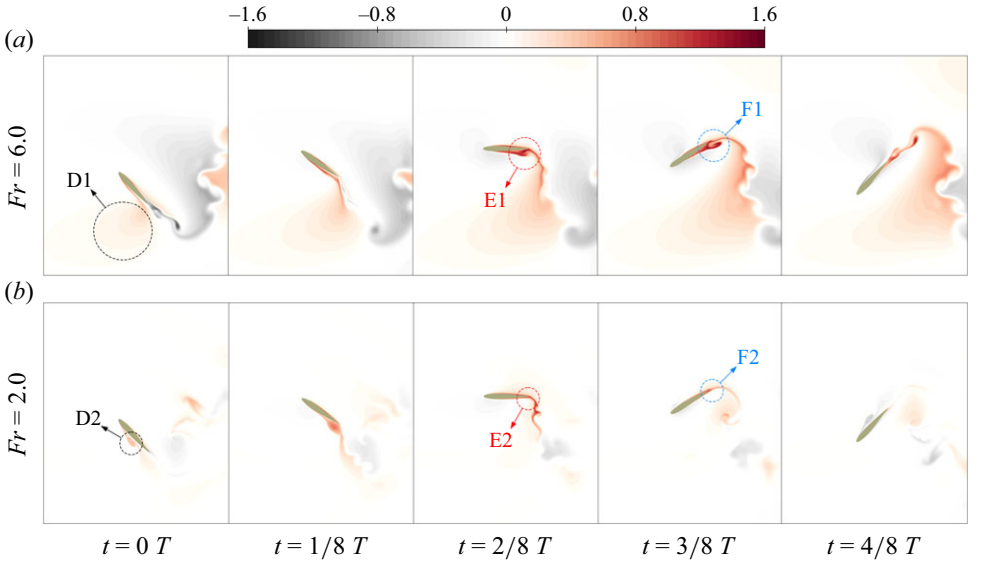


Figure 15. Evolution of instantaneous density field ρ' over the first half-oscillation cycle at $St = 0.60$ for (*a*) $Fr = 6.0$ and (*b*) $Fr = 2.0$. The regions highlighted by D1, E1 and F1 indicate the dominant inertial effects that drive density perturbation away from the foil at weak stratification, while the regions highlighted by D2, E2 and F2 indicate the dominant buoyancy effects that confine density perturbation to the vicinity of the foil at strong stratification.

the spreading of density perturbation encounters fewer barriers and covers a relatively large area of the fluid domain, as shown in figure 15(*a*). In contrast, the buoyancy effects that dominate the transport of density perturbation in strongly stratified fluids ($Fr = 2.0$) confine the disturbance to the vicinity of the oscillating foil (see figure 15*b*).

We further examine the instants of $t = 0T$ (approximating t_0), $t = 1/4T$ (t_1) and $t = 3/8T$ (t_2) in figure 15. At $t = 0T$, the dominant inertial effects facilitate the majority of density perturbation to spread away from the body at $Fr = 6.0$ (see D1 in figure 15*a*). However, the primary density spreading at $Fr = 2.0$ is restricted to regions near the body due to the dominance in buoyancy forces (see D2 in figure 15*b*). Similarly, at $t = 1/4T$ and $t = 3/8T$, the flow inertia in weakly stratified fluids induces a vertical stretching of density perturbation around the foil's trailing edge (E1 and F1 in figure 15*a*), which is flattened by buoyancy forces in strongly stratified fluids (E2 and F2 in figure 15*b*). These dynamical behaviours account for the observations in figure 14.

To provide some quantitative implications for the above discussion, we perform an analysis of instantaneous streamwise forces acting on the oscillating foil. We first run two separate simulations in stratified and homogeneous fluids, yielding total force F and its unstratified counterpart F_h, respectively. Then, the enhanced force resulting from density stratification can be obtained by $F_s = F - F_h$. Here, F_s can be used to characterise the force component arising from buoyancy effects, while F_h indicates the force component due to the rest of the effects. Figure 16 presents the comparison of force components between different stratifications at $St = 0.60$. As shown in figure 16(*a*), F is largely determined by F_h with negligible contribution from F_s at $Fr = 6.0$. As the stratification level increases to $Fr = 2.0$, F_s takes a considerable proportion in F (see figure 16*b*). Further decrease in Fr gives rise to the dominating F_s over F_h, as indicated in figure 16(*c*). This rising contribution of the buoyancy-induced component F_s to total force F confirms the increasing dominance of buoyancy effects in the dynamical behaviours of

https://doi.org/10.1017/jfm.2025.283 Published online by Cambridge University Press

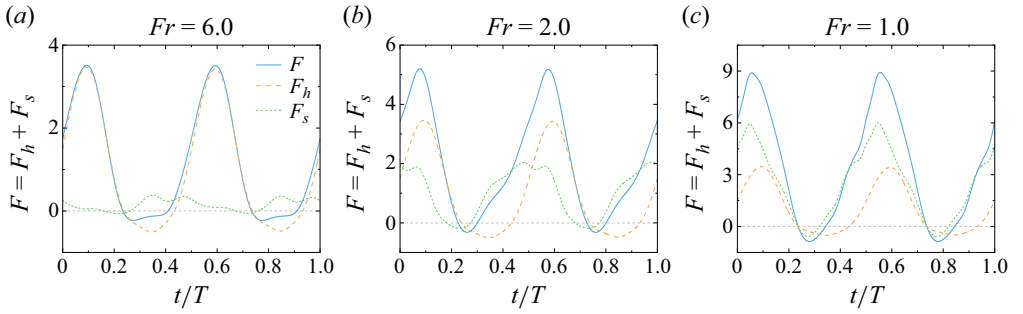


Figure 16. Instantaneous streamwise forces acting on the oscillating foil at $St = 0.60$ for (a) $Fr = 6.0$, (b) $Fr = 2.0$ and (c) $Fr = 1.0$. The total force F is split into two parts, i.e. F_s denoting the buoyancy-induced contribution and F_h denoting the contribution due to the rest of the effects. All forces are normalised by the time-averaged thrust over one oscillation cycle in homogeneous fluids.

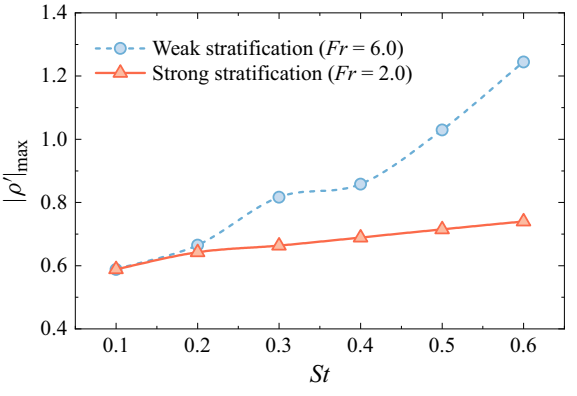


Figure 17. Variation of maximum density perturbation magnitude as a function of Strouhal number for different stratification strengths.

flow disturbance, in accordance with the observations in figure 15. It is worth mentioning that recent studies (Zhang *et al.* 2019; More *et al.* 2021) have proposed rigorous splitting methods to further disentangle the force due to stratification effects. We leave this for future studies.

During the fluid entrainment, increasing Strouhal number amplifies density transport. Figure 17 shows the maximum density perturbation magnitude at $t = T$ for different Strouhal numbers. The results indicate that, in weakly stratified fluids, the intensity of density motion increases nonlinearly with St, owing to the combined effects of flow inertia and buoyancy forces on density spreading. In strongly stratified fluids, however, a nearly linear increase in maximum density disturbance is observed as St becomes higher, with buoyancy effects exclusively governing density perturbation. The magnitude of density transport at $Fr = 6.0$ is notably higher than that at $Fr = 2.0$, especially for high Strouhal numbers. This behaviour is expected, as stronger stratifications provide greater resistance to vertical motions (Magnaudet & Mercier 2020; More & Ardekani 2023).

Figure 18 depicts the effect of the Strouhal number on the instantaneous density field at $t = T$. The direction and thickness of arrows illustrate the orientation and intensity of density spreading, respectively. We can see that stronger foil oscillations result in a wider scope of density transport. For $Fr = 6.0$, inertial effects convey the enhanced density perturbation towards regions far from the body as St increases, as shown by blue arrows in

https://doi.org/10.1017/jfm.2025.283 Published online by Cambridge University Press

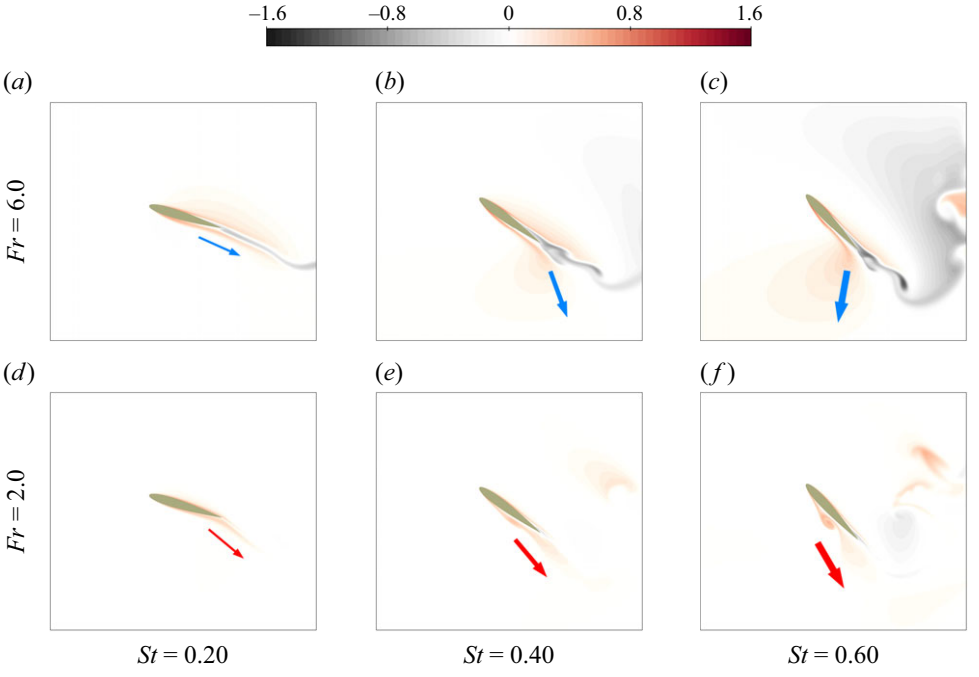


Figure 18. Influence of Strouhal number on instantaneous density field ρ' for $(a–c)$ $Fr = 6.0$ and $(d–f)$ $Fr = 2.0$. The spreading tendency and magnitude of density perturbation are illustrated by the direction and thickness of arrows.

figures 18(*a*)–18(*c*). By comparison, the significant buoyancy effects at $Fr = 2.0$, which promote the entrained fluids returning to their neutrally buoyant position, confine the amplifying density disturbance to the vicinity of the oscillating foil as St increases, as shown by red arrows in figures 18(*d*)–18(*f*). The amplification of density disturbance near the foil is beneficial to thrust production at this stage, as discussed in figures 11 and 14. However, when the foil approaches the drag-produced phase ($t_1 < t < t_2$), this St-induced amplification, sufficiently inhibited by pronounced buoyancy effects in strongly stratified fluids, becomes detrimental to thrust performance, as indicated in figures 12, 13 and 14. In summary, the strong stratifications can effectively capitalise on the amplification of density motion during the asymmetric fluid entrainment, which is a leading mechanism responsible for the notably high optimal St observed in strongly stratified fluids.

5. Stratification-induced wake dynamics

In addition to hydrodynamic performance, another aspect in which the Strouhal number plays an important role is the wake dynamics. It has been well documented that an oscillating foil with different Strouhal numbers can generate a wide variety of wake patterns in homogeneous fluids (Schnipper *et al.* 2009; Andersen *et al.* 2017; Verma & Hemmati 2022). In a stratified fluid, the baroclinic torque arising from isopycnal deflection can alter vorticity evolution, yielding flow patterns that differ from those in homogeneous fluids. Specifically, the wake structures under the stratification influence are governed by buoyancy effects, which inhibit the vertical motion while promoting the horizontal motion (Riley & Lelong 2000), and by induced internal waves that significantly impact the transport of energy and momentum (Staquet & Sommeria 2002). Given that the wake dynamics of oscillating foils in stratified regimes is largely unexplored, we provide an

https://doi.org/10.1017/jfm.2025.283 Published online by Cambridge University Press

analysis regarding the role of Strouhal number in the stratified wake behaviours in this section.

It should also be noted that, despite extensive efforts in correlating propulsive performance with flow features, the intrinsic relationship between them remains complex and often inconsistent. Godoy-Diana *et al.* (2008) observed that the wake transition from a typical von Kármán street, associated with drag generation, to a reverse von Kármán street, indicative of thrust production, precedes the drag–thrust transition. Smits (2019) further indicated that wake dynamics and propulsive performance should be treated as two distinct yet interrelated topics, because efficient swimming may correspond to multiple different wake patterns. Such perspective is echoed by Eloy (2012), Zhang (2017) and Taylor (2018), who suggested that efficient flow patterns are more likely to be a consequence of efficient propulsion, and caution should be exercised when employing wake development to explain propulsive performance. Therefore, rather than seeking to build a one-to-one connection between propulsive performance and wake structure, we mainly aim to map out the wake types across the $(St,\ Fr)$ plane and offer novel insights into flow patterns in stratified environments.

5.1. *Vortex structures*

As a basis for comparison, figure 19 shows the wake evolution of a harmonically heaving and pitching foil across different Strouhal numbers in a homogeneous fluid. From figure 19(a), we observe a 2P wake at $St = 0.10$, which transitions into a 2S reverse von Kármán wake as the Strouhal number increases to $St = 0.20$ (see figure 19b). According to the terminology by Williamson & Roshko (1988), 2P and 2S respectively denote two vortex pairs and two single vortices shed per oscillation cycle. As the Strouhal number further increases, the reverse von Kármán wake becomes more coherent in its spatial arrangement, as depicted in figure 19(c–f). These typical wake patterns are commonly observed in both experimental measurements and numerical simulations of homogeneous fluids (Schnipper *et al.* 2009; Andersen *et al.* 2017).

Figure 20 presents the evolution of wake configuration with St in a weakly stratified fluid ($Fr = 6.0$). Due to the generation of internal waves, the consecutive wave beams are evident in the flow pattern around the oscillating foil. When foil motion is weak, the wake pattern is characterised by a dispersed configuration, as shown in figure 20(a). As the Strouhal number increases, the flow pattern evolves into a structure consisting of a central wake moving along the centreline and two symmetric oblique wakes deflecting outward (see figure 20b,c). Further increase in the Strouhal number leads to the merging of the central and oblique wakes, resulting in a chaotic flow pattern behind the oscillating foil, as illustrated in figure 20(d–f). In addition, the wake configuration in weakly stratified fluids shows a downstream tendency due to the dominance of the free stream over the propagation of induced internal waves.

The variation of wake structures with St in a strongly stratified fluid ($Fr = 2.0$) is exhibited in figure 21. Notably, the flow pattern undergoes a transition from an asymmetric arrangement at low Strouhal numbers to a symmetric configuration at high Strouhal numbers. The prominence of internal waves also increases with the strength of stratification. The growing influence of internal waves prompts vortex disturbances to spread towards the upstream region, giving rise to a radial flow pattern in strongly stratified conditions. The formation of wake patterns in a stratified regime depends on several factors, including the foil–vortex interplay, the vortex–vortex intertwining, and the interaction between internal waves and background mean flow. Especially, the wave–mean flow interaction, which irreversibly transfers energy to smaller scales, plays a critical role

https://doi.org/10.1017/jfm.2025.283 Published online by Cambridge University Press

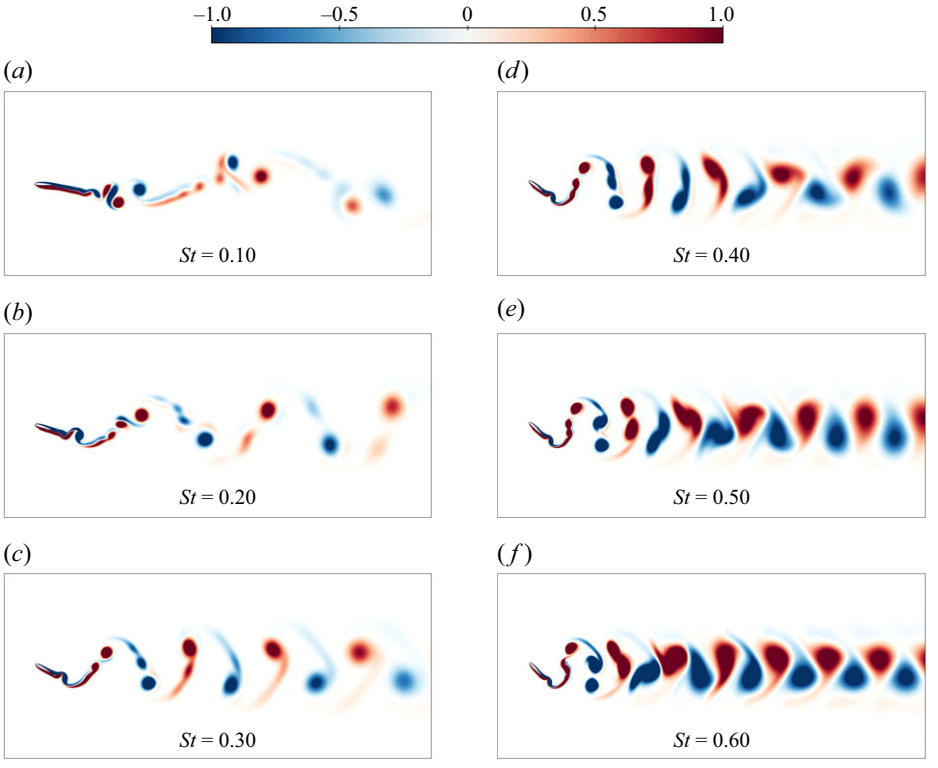


Figure 19. Instantaneous vorticity contours, normalised by U_∞/c, at (*a*) $St = 0.10$, (*b*) $St = 0.20$, (*c*) $St = 0.30$, (*d*) $St = 0.40$, (*e*) $St = 0.50$ and (*f*) $St = 0.60$ for a homogeneous fluid ($Fr = \infty$). The flow pattern in a homogeneous fluid experiences a typical transition from 2P wake to 2S wake with the Strouhal number.

in the wake dynamics of stratified fluids (Staquet & Sommeria 2002; Howland *et al.* 2021). Both stronger foil motion and increasing stratification strength facilitate this process. Consequently, at high Strouhal numbers and low Froude numbers, the near wake becomes considerably disordered, as seen in figure 21(*f*). Our previous study (Wang *et al.* 2024), which focused on $St = 0.30$, provided a detailed illustration on the formation process of wake patterns in a stratified fluid medium.

It can also be seen from figures 20 and 21 that the inhomogeneous background density distribution does not change the general wake symmetry about the centreline. For a linearly stratified fluid governed by Boussinesq equations, the density perturbation only depends on the background density gradient γ, as illustrated by (2.10). Because γ is constant throughout the whole domain, there is no dynamical distinction between upward and downward density perturbations (Sutherland 2010). Consequently, the flow patterns retain an overall symmetry about the centreline. Such symmetric wakes about the horizontal axis in a linearly stratified fluid have been widely observed by both numerical simulations and experimental measurements (Chongsiripinyo *et al.* 2017; Madison *et al.* 2022; Ortiz-Tarin *et al.* 2023). However, due to the distortion of vortex structures by stratification effects, conventional wake classification symbols introduced by Williamson & Roshko (1988) are inadequate for describing wake types in stratified fluids. In this study, we classify wake types based on the spatial extent and concentration regions of vortex disturbances. As shown in figure 22, five representative flow patterns are identified within the parameter space defined by St and Fr.

https://doi.org/10.1017/jfm.2025.283 Published online by Cambridge University Press

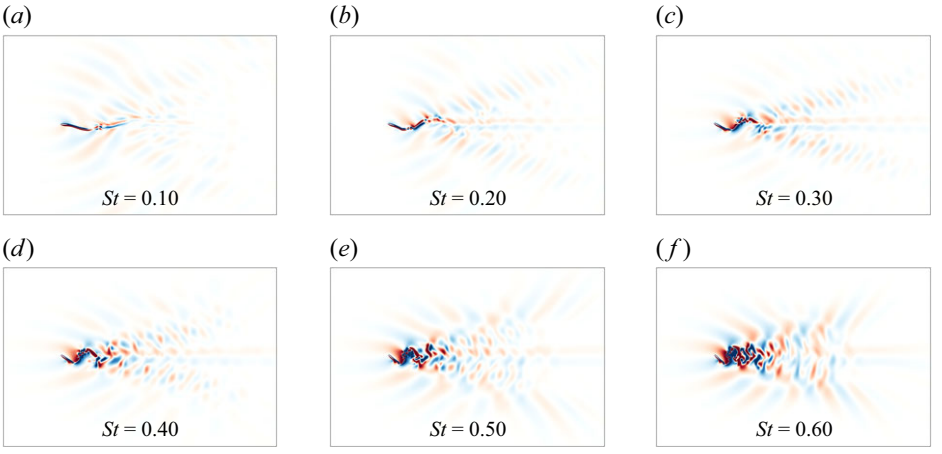


Figure 20. Instantaneous vorticity contours at (a) $St = 0.10$, (b) $St = 0.20$, (c) $St = 0.30$, (d) $St = 0.40$, (e) $St = 0.50$ and (f) $St = 0.60$ for a weakly stratified fluid ($Fr = 6.0$). Contour colours are the same as in figure 19. The flow pattern in a weakly stratified fluid exhibits a downstream tendency.

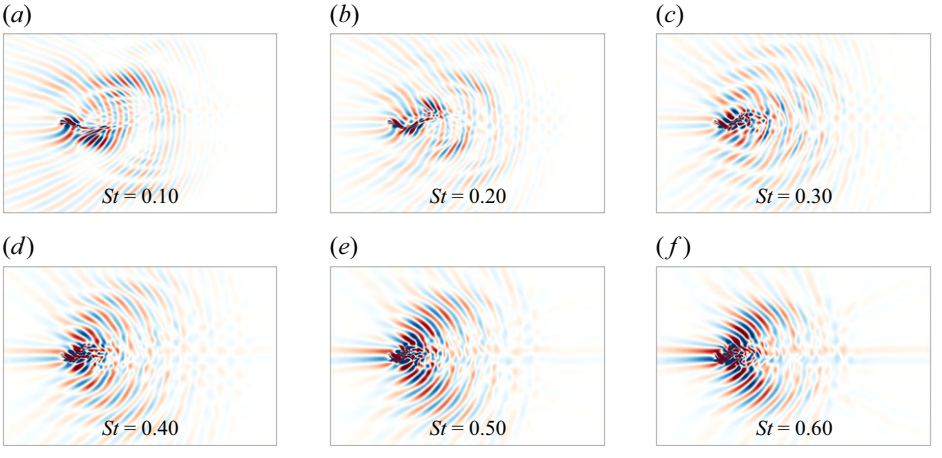


Figure 21. Instantaneous vorticity contours at (a) $St = 0.10$, (b) $St = 0.20$, (c) $St = 0.30$, (d) $St = 0.40$, (e) $St = 0.50$ and (f) $St = 0.60$ for a strongly stratified fluid ($Fr = 2.0$). Contour colours are the same as in figure 19. The flow pattern in a strongly stratified fluid exhibits a radial tendency.

Flow pattern I is characterised by a radial configuration centred on the oscillating foil, with primary vortex disturbance concentrated around the body (figure 22a). Flow pattern II presents the vorticity concentration only appearing in the downstream region behind the foil's leading edge (figure 22b). Flow pattern III exhibits a shuttle shape in which vorticity concentrates along the centreline both upstream and downstream (figure 22c). Pattern IV is similar to pattern III but features a bifurcated downstream vortex concentration, leading to a larger vertical scale (figure 22d). Flow pattern V displays a triangular configuration, with vortex disturbance aggregating downstream (figure 22e). In addition, stratification effects induce a symmetry breaking in the wake as St and Fr vary. Figure 22(f) contrasts asymmetric and symmetric wakes under these conditions.

Figure 23 provides a map of flow patterns in the (St, Fr) plane. The regime with low Fr is dominated by flow pattern I, due to the significant influence of induced internal waves. As stratification weakens, the Strouhal number starts to play a comparable role in

https://doi.org/10.1017/jfm.2025.283 Published online by Cambridge University Press

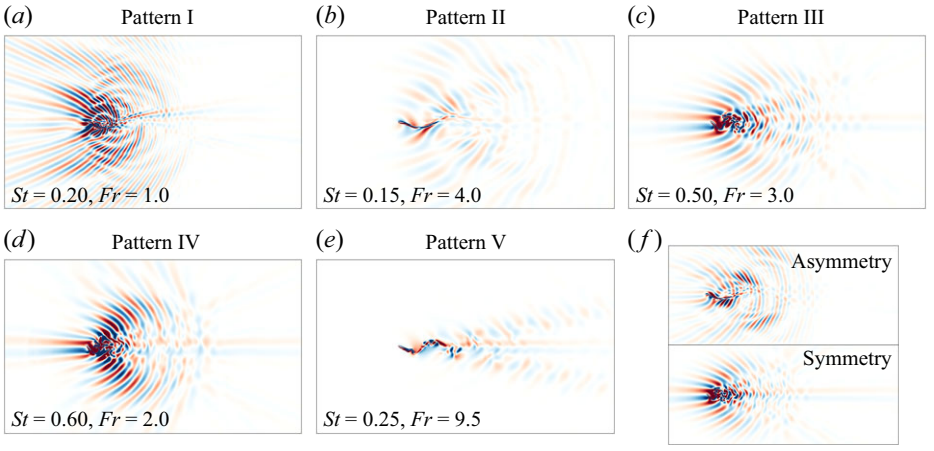


Figure 22. (*a–e*) Instantaneous vorticity contours showing typical flow patterns generated by an oscillating foil in stratified fluids. (*f*) Comparison between asymmetric ($St = 0.15$, $Fr = 2.0$) and symmetric ($St = 0.60$, $Fr = 3.0$) wakes behind an oscillating foil in stratified fluids. Contour colours are the same as in figure 19.

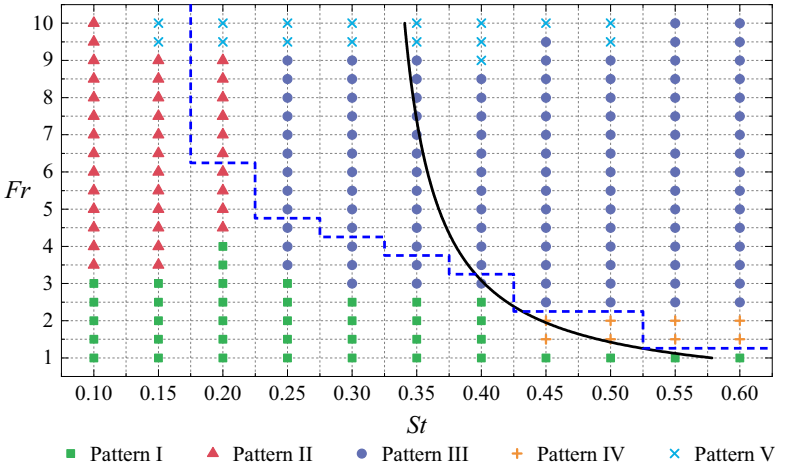


Figure 23. Flow pattern map for an oscillating foil in stratified fluids. The pattern types correspond to the vorticity contours in figure 22. The blue dashed line indicates the wake transition from asymmetry (lower-left regime) to symmetry (upper-right regime). The black solid line corresponds to the optimal Strouhal numbers at different levels of stratification.

wake evolution. As a result, the regime with $St \leqslant 0.20$ is represented by flow pattern II, while pattern III occupies the regime with $St > 0.20$. The combination of intense foil motion (high St) and strong stratification (low Fr) leads to an isolated regime in the lower-right corner of the wake map, characterised by flow pattern IV. Another distinct regime, defined by high Fr and moderate St, corresponds to flow pattern V, resulting from the dominant influence of background mean flow under extremely weak stratifications.

The blue dashed line in figure 23 separates the flow pattern map into a lower-left regime, where asymmetric wakes dominate, and an upper-right regime, where symmetric wakes prevail. Generally, weak foil motion coupled with strong stratification tends to break wake symmetry, while higher Fr and St values favour the formation of symmetric wakes. These results are expected to offer a phase diagram of wake characteristics in stratified

https://doi.org/10.1017/jfm.2025.283 Published online by Cambridge University Press

environments, enabling a comparison with homogeneous observations (Godoy-Diana *et al.* 2008; Schnipper *et al.* 2009; Andersen *et al.* 2017).

Figure 23 also illustrates the variation of optimal Strouhal numbers in the $(St,\ Fr)$ plane, as indicated by the black solid line. For weak stratifications, the optimum efficiency is observed at a higher St than the value of wake transition. This observation is consistent with the previous study on an oscillating foil in homogeneous fluids (Deng *et al.* 2016). However, in strongly stratified fluids, we find that the optimal condition of efficiency performance aligns with the wake transition point, indicating a synchronisation between the foil's kinematics and flow disturbances. This behaviour presumably echoes earlier discussion regarding the inherent coupling between oscillatory frequency of the foil and Brunt–Väisälä frequency of stratified fluids.

One of the most striking features of flow patterns produced by a moving body in a stably stratified fluid is the presence of internal waves, as shown in figures 20–22. Lighthill (1967) developed a general theory that describes the generation of anisotropic dispersive waves by travelling disturbances. Stevenson & Thomas (1969) performed a series of experiments on internal wave patterns induced by a horizontally moving cylinder with forced oscillation and found that their results are in good agreement with Lighthill's theory. Subsequent studies by Rehm & Radt (1975) and Voisin (1994) further confirmed the validity of Lighthill's theory in predicting internal wave patterns generated by translating and oscillating sources.

Here, we compare the internal wave patterns obtained from our numerical simulations with the predictions of Lighthill's theory, as shown in figure 24. Specifically, we examine the case of $Fr = 8.0$ with a constant Brunt–Väisälä frequency and body velocity. By varying the oscillatory frequency of the foil, we analyse two distinct scenarios: $\Omega < 1$ ($\Omega = 0.402$) and $\Omega > 1$ ($\Omega = 1.608$). For a translating body with forced oscillation, the wave system induced by the oscillation is superimposed on the steady wave system, which remains stationary relative to the oscillatory source (Stevenson & Thomas 1969). According to Lighthill's theory, the wave system generated by steady motion consists of a series of semicircles centred on the body, whereas the oscillatory wave system exhibits different patterns depending on Ω. When $\Omega < 1$, the oscillatory wave system displays a radial pattern propagating both upstream and downstream. In contrast, when $\Omega > 1$, this system transitions into a wedge-shaped pattern trailing behind the oscillating body. Both the radial wave pattern (figure 24*b*) and the wedge-shaped wave pattern (figure 24*d*) are accurately captured in the simulations (figure 24*a*,*c*). Notably, the wave spacing observed in our numerical simulations aligns closely with theoretical predictions.

Despite this agreement, certain discrepancies are evident between the two results. The vortex shedding from the trailing edge of the foil in the simulations induces chaotic wave patterns in the downstream region near the body, which are absent in the theoretical predictions. Additionally, the numerical wave patterns along the centreline exhibit significant distortion, which notably deviates from theoretical expectations. This discrepancy arises because nonlinear effects, such as wave interactions and wave breaking, are not fully captured by Lighthill's theory, which is based on linear assumptions. In contrast, our numerical simulations inherently account for these nonlinear phenomena.

5.2. *Velocity profiles*

We further investigate the velocity distribution in stratified fluids. Figure 25 compares the contours of time-averaged streamwise velocity between homogeneous and stratified cases. In the homogeneous case (figure 25*a*), the mean velocity field displays an energetic momentum jet behind the oscillating foil, generated by the reverse von Kármán vortex

https://doi.org/10.1017/jfm.2025.283 Published online by Cambridge University Press

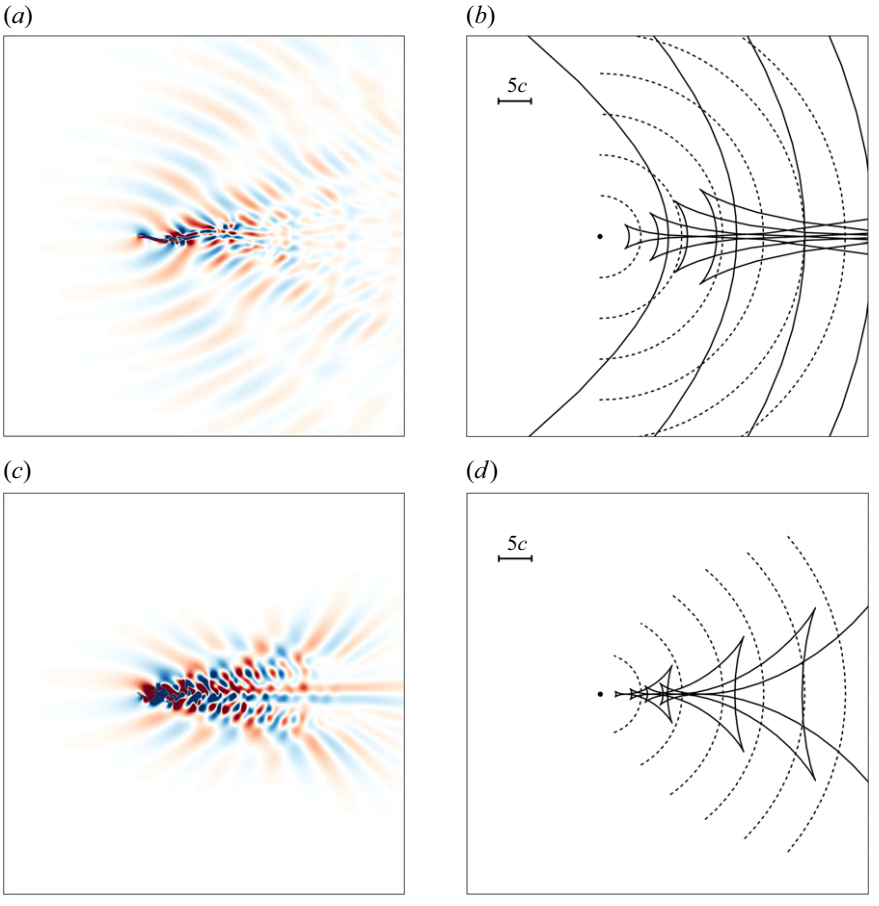


Figure 24. Comparison of internal wave patterns between numerical simulations and theoretical predictions at $Fr = 8.0$: (a) and (b) $\Omega = 0.402$, and (c) and (d) $\Omega = 1.608$. The simulations in panels (a) and (c) show the vorticity field, normalised by U_∞/c with the range from -0.2 to 0.2. The predictions by Lighthill's theory (Lighthill 1967) presented in panels (b) and (d) show the curves of constant phase for internal waves (such as wave crests), in which the dashed lines represent the wave system from steady motion ($\Omega = 0$) and the solid lines depict waves induced by oscillation.

street (figure 19). As St increases, a noticeable intensification in both magnitude and scope is observed in the near-wake jet. At the highest Strouhal number studied ($St = 0.60$), the momentum jet exhibits a tendency of bifurcation in the vicinity of the foil. Note that the velocity jet is typically considered as a key indicator of thrust production in homogeneous studies (Dewey *et al.* 2012; Quinn *et al.* 2014; Verma & Hemmati 2022).

Figures 25(b) and 25(c) show the time-averaged velocity contours in weakly and strongly stratified fluids, respectively. In these stratified conditions, the velocity distribution is characterised by a central momentum excess region flanked by diverging velocity streams. These streams are noted to follow the pattern of internal waves, manifesting as alternating velocity excess and deficit streaks. Similar to the homogeneous case, stronger foil motion results in more energetic momentum jets in stratified fluids. Notably, the presence of internal waves induces a significant bifurcation in the central jet at $St = 0.60$. For weak stratification, this bifurcated jet is interrupted by a velocity deficit region, as seen in figure 25(b). In contrast, under strong stratification, the velocity deficit region splits the jet along the centreline into two streams near the foil, which eventually merge into a

https://doi.org/10.1017/jfm.2025.283 Published online by Cambridge University Press

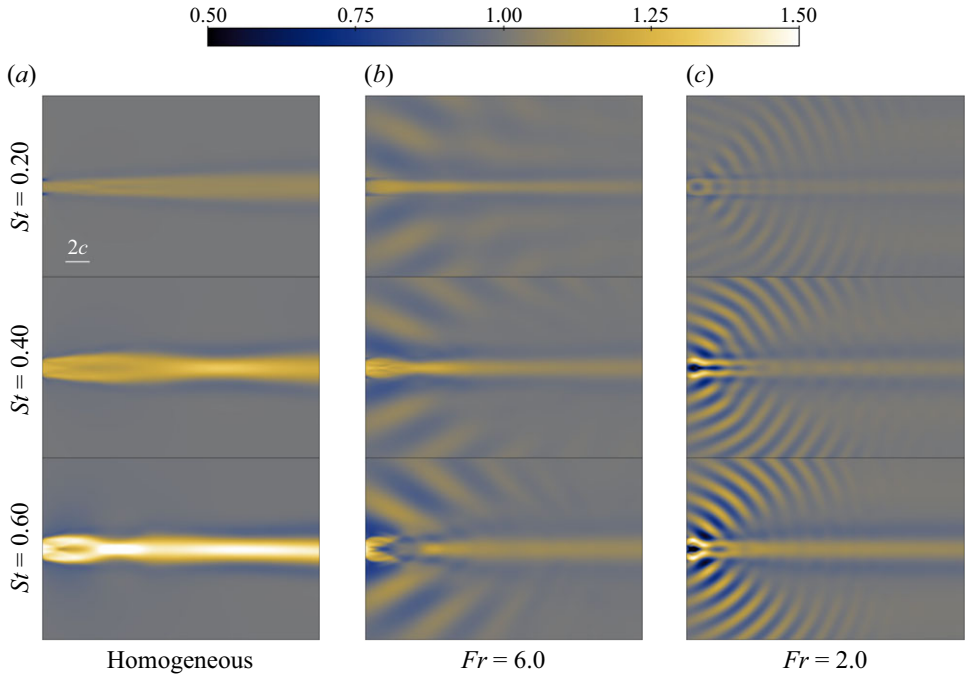


Figure 25. Contours of time-averaged streamwise velocity, normalised by the free stream velocity U_∞, at varying Strouhal numbers for (*a*) $Fr = \infty$ (homogeneous case), (*b*) $Fr = 6.0$ and (*c*) $Fr = 2.0$. The initial position of the foil's trailing edge is located at the left boundary of each plot.

single jet further downstream (figure 25*c*). This difference is attributed to varying wave frequencies in weakly and strongly stratified fluids. The central momentum jet under weak stratification is comparable to that in the homogeneous case, but only near the foil's trailing edge. Given the similar level of thrust production between weakly stratified and homogeneous cases (figure 5*a*), it suggests that the near-wake velocity jet is a more pivotal indicator of thrust performance, while far-wake velocity distribution is less significant. Interestingly, the central momentum jet in strongly stratified fluids is less energetic than that in homogeneous fluids, despite the higher thrust production at $Fr = 2.0$ compared with $Fr = \infty$ (figure 5*a*). This implies that diverging velocity excess streams also contribute to thrust production, and these wave-induced velocity streaks must be fully considered when evaluating thrust through streamwise momentum flux.

We also quantitatively assess the mean velocity profiles in figures 26–28, focusing on the cross-stream line at five streamwise locations. The near-wake region is characterised by $x/c = 0.5$, $x/c = 1.0$, $x/c = 2.0$ and $x/c = 3.0$, while $x/c = 10.0$ represents the far wake. In the homogeneous case (figure 26), the central jet with multiple velocity peaks dominates the wake, consistent with the observations in figure 25(*a*). Additionally, low Strouhal numbers cause wake bifurcation in the far wake (figure 26*e*), whereas strong foil motion leads to bifurcation in the near wake (figure 26*a–d*). In stratified regimes, the mean velocity distribution along the cross-stream line exhibits a wavy profile, with central primary peaks flanked by alternating minima and maxima (figures 27 and 28). These velocity minima and maxima, which decay downstream or away from the centreline, mirror the diverging velocity deficit and excess streams in figures 25(*b*) and 25(*c*). We see that the bifurcation of velocity distribution under stratification only occurs in the near wake. More specifically, the central velocity profile at weak stratification tends to bifurcate when St exceeds a

https://doi.org/10.1017/jfm.2025.283 Published online by Cambridge University Press

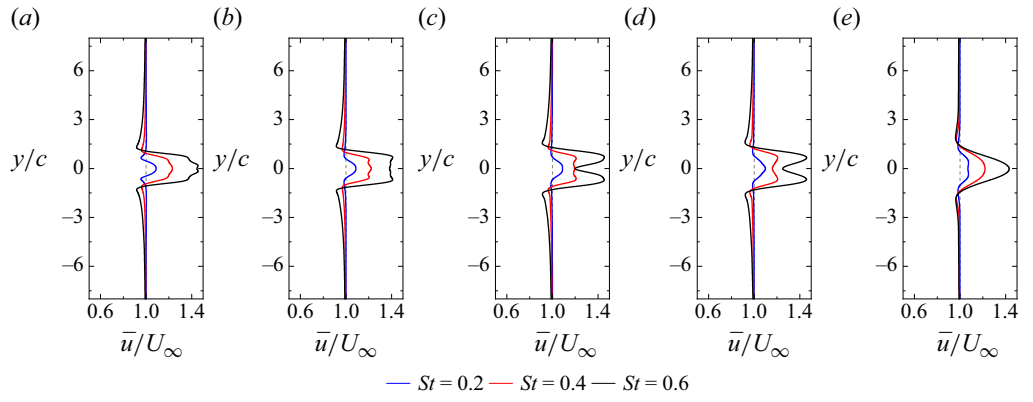


Figure 26. Time-averaged streamwise velocity profiles with varying Strouhal numbers along the cross-stream line at streamwise locations of (*a*) $x/c = 0.5$, (*b*) $x/c = 1.0$, (*c*) $x/c = 2.0$, (*d*) $x/c = 3.0$ and (*e*) $x/c = 10.0$ downstream of foil trailing edge for a homogeneous fluid ($Fr = \infty$).

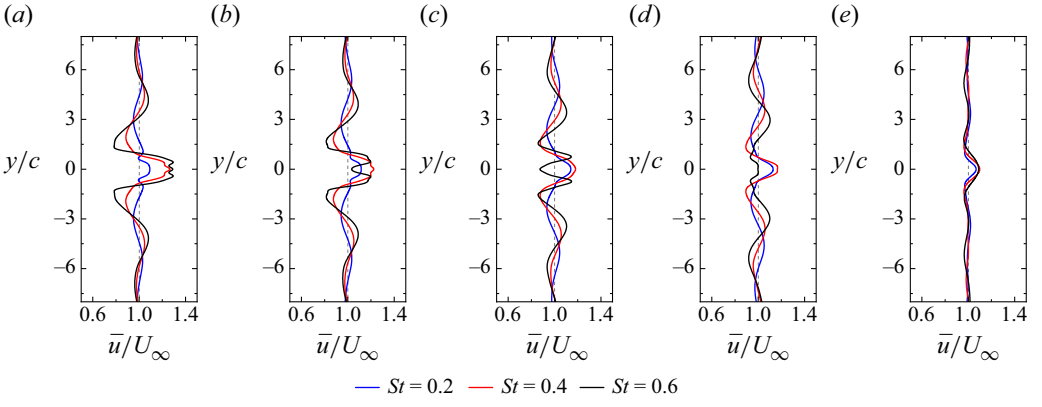


Figure 27. Time-averaged streamwise velocity profiles with varying Strouhal numbers along the cross-stream line at streamwise locations of (*a*) $x/c = 0.5$, (*b*) $x/c = 1.0$, (*c*) $x/c = 2.0$, (*d*) $x/c = 3.0$ and (*e*) $x/c = 10.0$ downstream of foil trailing edge for a weakly stratified fluid ($Fr = 6.0$).

certain value, resembling the behaviour in homogeneous fluids (figure 27*a–d*). In contrast, strong stratification consistently induces bifurcation along the centreline, independent of St (figure 28*a–d*).

As previously noted, increasing the Strouhal number significantly enhances the momentum jet behind the oscillating foil. However, this velocity enhancement manifests differently in homogeneous and stratified fluids. In the homogeneous case, the enhanced momentum flux is directed downstream, resulting in a uniform velocity distribution along the centreline (figure 25*a*). Conversely, the stratification effects tend to concentrate the intensified momentum flux upstream, creating highly energetic velocity excess streams near the foil (see figures 25*b* and 25*c*). The quantitative results presented in figures 26–28 further confirm this behaviour. It is apparent from figure 26 that the peaks of velocity profiles in a homogeneous fluid consistently depend on the Strouhal number along the centreline. In stratified regimes, however, the variation of mean velocity profiles with the Strouhal number is evident only in the near wake, while the minima and maxima of velocity in the far wake are nearly independent of the Strouhal number (figures 27 and 28).

https://doi.org/10.1017/jfm.2025.283 Published online by Cambridge University Press

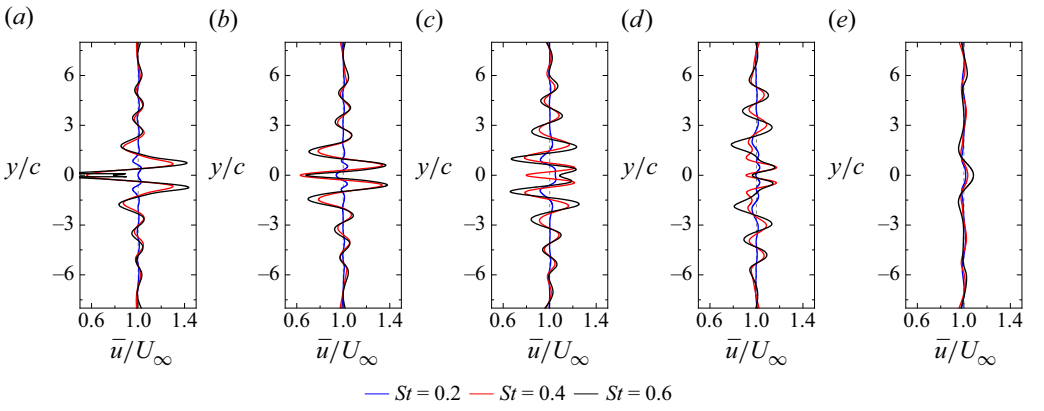


Figure 28. Time-averaged streamwise velocity profiles with varying Strouhal numbers along the cross-stream line at streamwise locations of (*a*) $x/c = 0.5$, (*b*) $x/c = 1.0$, (*c*) $x/c = 2.0$, (*d*) $x/c = 3.0$ and (*e*) $x/c = 10.0$ downstream of foil trailing edge for a strongly stratified fluid ($Fr = 2.0$).

More importantly, we observe a more energetic near wake at $Fr = 2.0$ compared with that of $Fr = 6.0$, indicating an increased concentration of momentum flux with stronger stratification. This behaviour partly explains the significant thrust production and the notably high optimal Strouhal numbers in strongly stratified fluids.

6. Conclusions

This study numerically investigates the Strouhal number dependence of propulsive performance for a combined heaving and pitching foil in density stratified fluids. The results demonstrate that the optimal Strouhal number St_m is significantly influenced by stratification strength. For weak stratifications ($Fr \geqslant 5$), the highest efficiency occurs at a Strouhal number similar to that observed in homogeneous fluids. However, as stratification strengthens ($Fr < 5$), the optimal Strouhal number increases with decreasing Fr, eventually exceeding the typical range of $0.20 < St < 0.40$ observed in homogeneous conditions. Notably, the strongest stratification in our parameter space yields an optimal Strouhal number of $St_m = 0.59$, significantly higher than those observed in homogeneous fluids. Our findings suggest an inherent coupling between oscillatory frequency of the foil and the Brunt–Väisälä frequency of the fluid. The highest efficiency in oscillatory propulsion occurs when resonance between the foil and fluid oscillations is triggered. A fitting formula based on this hypothesis accurately characterises the relationship between St_m and Fr, indicating that resonance behaviour is a key factor driving the increase in St_m with stratification strength.

We further explore the hydrodynamic mechanisms underlying these observations. The results reveal that asymmetric fluid entrainment by foil oscillation plays a crucial role in achieving high optimal Strouhal numbers under strong stratifications. The oscillating foil drags a volume of fluid into regions with varying densities, inducing density perturbations governed by the relative magnitudes of inertial and buoyancy effects. In weakly stratified fluids, flow inertia tends to direct the density disturbances away from the foil, while in strongly stratified fluids, buoyancy forces restrict density transport to regions close to the foil. During fluid entrainment, increasing the Strouhal number facilitates density motion and amplifies density perturbations. We find that strong stratifications, associated with prominent buoyancy effects, can effectively exploit this St-induced enhancement

https://doi.org/10.1017/jfm.2025.283 Published online by Cambridge University Press

in density transport to create specific pressure distributions that benefit hydrodynamic performance. Consequently, in strongly stratified fluids, the streamwise component of instantaneous forces experiences a significant increase in peaks without a corresponding rise in drag generation as the Strouhal number increases. This behaviour contributes to a considerable improvement in cycle-averaged thrust production with increasing St, leading to efficient propulsion at higher Strouhal numbers.

The wake dynamics of an oscillating foil in stratified regimes is another focus in this study. We first provide a map of flow patterns by identifying various wake types in the (St, Fr) plane. It is noted that in weakly stratified fluids, the optimal Strouhal numbers tend to precede the values of wake transition, consistent with previous observations in homogeneous cases. Interestingly, the optimal condition at strong stratifications agrees well with the wake transition, distinguishing it from the homogeneous observations. We then explore the streamwise velocity features under the effects of stratification. Unlike the uniform distribution of the velocity jet in homogeneous fluids, stratification effects concentrate the enhanced momentum flux to approach the oscillating foil at higher St, resulting in highly energetic velocity excess streams in the near wake.

The findings of this study provide several new insights into oscillatory propulsion. First of all, some canonical optimisation procedures for homogeneous scenarios may not be applicable in stratified environments due to different optimal conditions. It is thus suggested that aquatic animals or artificial propulsors using oscillatory mechanisms should adopt different propulsion strategies to achieve efficient swimming in density stratified fluids. Additionally, an oscillating foil propulsor in strongly stratified fluids can attain optimum efficiency combined with considerable thrust production, avoiding the trade-off between thrust and efficiency commonly encountered in homogeneous cases. Moreover, the influence of stratification should be fully taken into consideration when using simple rules of thumb based on optimal Strouhal numbers to predict the cruising speed of aquatic animals. In this context, we retain the possibility that the presence of density stratification contributes to the surprisingly large Strouhal numbers observed in several natural swimmers, as oceans are inherently stratified.

Funding. This research has been supported by the Zhejiang Provincial Natural Science Foundation of China under Grant No. LZ25A020003 and the National Natural Science Foundation of China (Grants No. 92252102 and No. 92152109).

Declaration of interests. The authors report no conflict of interest.

Appendix. Verification of temporal and spatial independence

A sensitivity study is conducted to demonstrate the time, grid and domain independence of the computational code used in this study. Here, we consider the most extreme case with the strongest foil motion ($St = 0.6$) and highest stratification strength ($Fr = 1.0$) in the current parameter space.

Time sensitivity is first assessed by testing four different time steps: $\Delta t_1 = T/1000$, $\Delta t_2 = T/2000$, $\Delta t_3 = T/4000$ and $\Delta t_4 = T/8000$. Figure 29 shows the time histories of the instantaneous thrust and lift coefficients at different temporal resolutions. The results are found to be insensitive to temporal resolution when the number of time steps per oscillation cycle exceeds 4000. The temporal resolution of $\Delta t_3 = T/4000$ is therefore used to run all the simulations in the present study. We then assess the grid sensitivity. By varying the number of grid points on the foil surface and modifying the normal grid spacing, we examine four spatial resolutions: Grid 1 with 122 074 elements, Grid 2 with 203 481 elements, Grid 3 with 343 105 elements and Grid 4 with 574 553 elements.

https://doi.org/10.1017/jfm.2025.283 Published online by Cambridge University Press

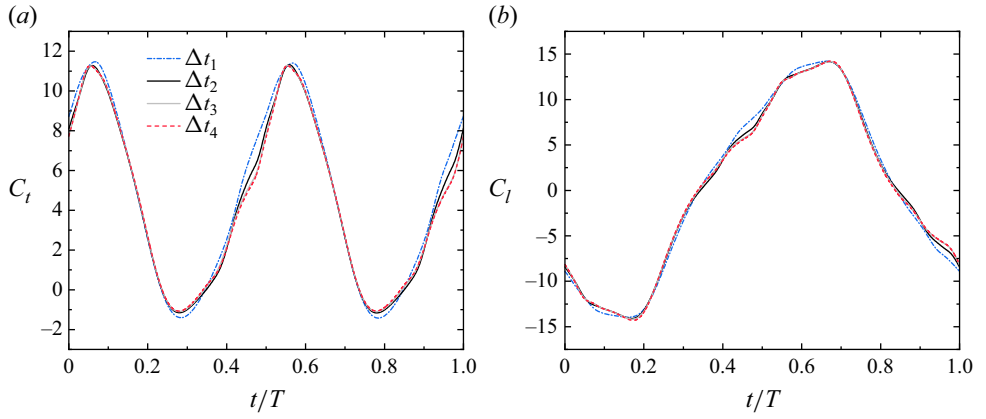


Figure 29. Time series of the instantaneous (*a*) thrust coefficient and (*b*) lift coefficient at $St = 0.6$ for $Fr = 1.0$ showing temporal independence by different time step resolutions.

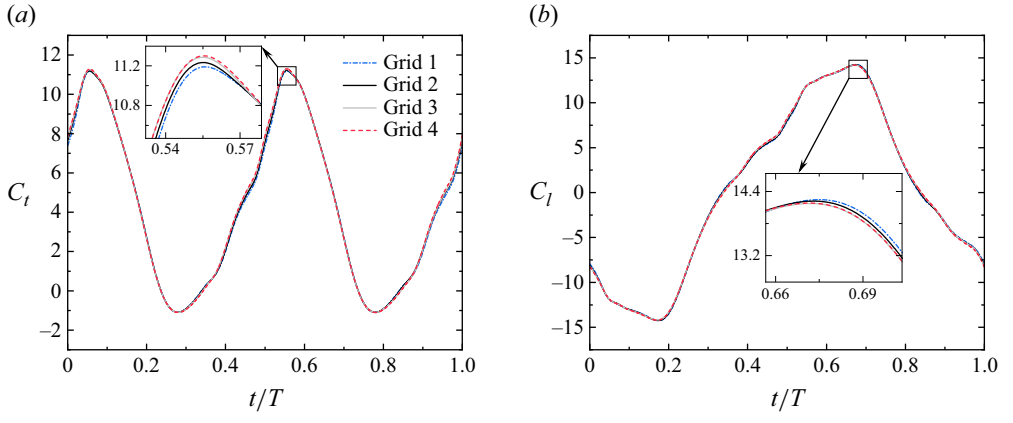


Figure 30. Time series of the instantaneous (*a*) thrust coefficient and (*b*) lift coefficient at $St = 0.6$ for $Fr = 1.0$ showing spatial independence by different grid resolutions.

The time series of force coefficients, as shown in figure 30, indicate excellent agreement between Grid 3 and Grid 4 with the largest deviation being less than 0.5 %. Therefore, we use spatial resolution Grid 3 to perform all the computations due to its satisfactory accuracy in space.

For numerical simulations of stratified fluids, the computational domain needs to be large enough to avoid the interactions between body and waves reflected from the boundaries. Here, we test four domain sizes to verify the independence of the computational domain. Figure 31 shows the force variations using the domain sizes $50c \times 50c$, $100c \times 100c$, $150c \times 150c$ and $200c \times 200c$, respectively. The maximum difference between the domain sizes $100c \times 100c$ and $150c \times 150c$ is 1.72 % in the instantaneous thrust coefficient C_t and 0.85 % in the instantaneous lift coefficient C_l. The deviation in the cycle-averaged thrust coefficient C_T between the domain sizes $50c \times 50c$ and $100c \times 100c$ is 5.22 %, which decreases to 1.79 % when comparing the domain sizes $100c \times 100c$ and $150c \times 150c$. Considering the trade-off between accuracy and computational cost, we select the domain size $100c \times 100c$ for all cases in this study.

https://doi.org/10.1017/jfm.2025.283 Published online by Cambridge University Press

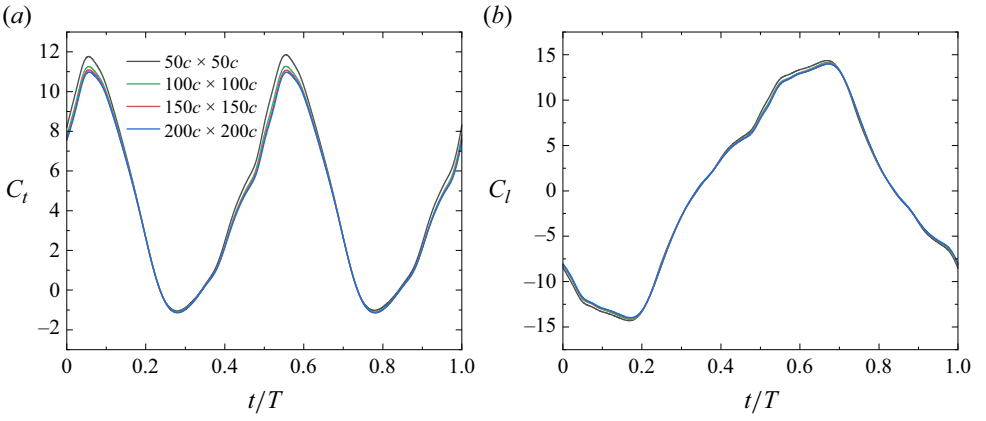


Figure 31. Time series of the instantaneous (*a*) thrust coefficient and (*b*) lift coefficient at $St = 0.6$ for $Fr = 1.0$ showing domain independence by different domain sizes.

References

Akiyama, S., Waki, Y., Okino, S. & Hanazaki, H. 2019 Unstable jets generated by a sphere descending in a very strongly stratified fluid. *J. Fluid Mech.* **867**, 26–44.

Alben, S. 2008 Optimal flexibility of a flapping appendage in an inviscid fluid. *J. Fluid Mech.* **614**, 355–380.

Alben, S. 2021 Collective locomotion of two-dimensional lattices of flapping plates. Part 2. Lattice flows and propulsive efficiency. *J. Fluid Mech.* **915**, A21.

Allshouse, M.R., Lee, F.M., Morrison, P.J. & Swinney, H.L. 2016 Internal wave pressure, velocity, and energy flux from density perturbations. *Phys. Rev. Fluids* **1** (1), 014301.

Andersen, A., Bohr, T., Schnipper, T. & Walther, J.H. 2017 Wake structure and thrust generation of a flapping foil in two-dimensional flow. *J. Fluid Mech.* **812**, R4.

Anderson, J.M., Streitlien, K., Barrett, D.S. & Triantafyllou, M.S. 1998 Oscillating foils of high propulsive efficiency. *J. Fluid Mech.* **360**, 41–72.

Ardekani, A.M. & Stocker, R. 2010 Stratlets: low Reynolds number point-force solutions in a stratified fluid. *Phys. Rev. Lett.* **105** (8), 084502.

Ardekani, A.M., Doostmohammadi, A. & Desai, N. 2017 Transport of particles, drops, and small organisms in density stratified fluids. *Phys. Rev. Fluids* **2** (10), 100503.

Arntsen, Ø.A. 1996 Disturbances, lift and drag forces due to the translation of a horizontal circular cylinder in stratified water. *Exp. Fluids* **21** (5), 387–400.

Buchholz, J.H.J. & Smits, A.J. 2008 The wake structure and thrust performance of a rigid low-aspect-ratio pitching panel. *J. Fluid Mech.* **603**, 331–365.

Chongsiripinyo K., Pal A. & Sarkar S. 2017 On the vortex dynamics of flow past a sphere at Re = 3700 in a uniformly stratified fluid. *Phys. Fluids* **29** (2), 020704.

Christin, S., Meunier, P. & Le Dizès, S. 2021 Fluid–structure interactions of a circular cylinder in a stratified fluid. *J. Fluid Mech.* **915**, A97.

Deng, J. & Caulfield, C.P. 2016 Dependence on aspect ratio of symmetry breaking for oscillating foils: implications for flapping flight. *J. Fluid Mech.* **787**, 16–49.

Deng, J. & Caulfield, C.P. 2018 Horizontal locomotion of a vertically flapping oblate spheroid. *J. Fluid Mech.* **840**, 688–708.

Deng J. & Kandel P. 2022 Drag force on a circular cylinder in stratified flow: a two-dimensional numerical study. *Phys. Fluids* **34** (5), 056601.

Deng, J., Sun, L., Teng, L., Pan, D. & Shao, X. 2016 The correlation between wake transition and propulsive efficiency of a flapping foil: a numerical study. *Phys. Fluids* **28** (9), 094101.

Dewey, P.A., Carriou, A. & Smits, A.J. 2012 On the relationship between efficiency and wake structure of a batoid-inspired oscillating fin. *J. Fluid Mech.* **691**, 245–266.

Dong, H., Mittal, R. & Najjar, FM 2006 Wake topology and hydrodynamic performance of low-aspect-ratio flapping foils. *J. Fluid Mech.* **566**, 309–343.

Doostmohammadi, A., Dabiri, S. & Ardekani, A M. 2014 A numerical study of the dynamics of a particle settling at moderate Reynolds numbers in a linearly stratified fluid. *J. Fluid Mech.* **750**, 5–32.

Eloy, C. 2012 Optimal Strouhal number for swimming animals. *J. Fluid. Struct.* **30**, 205–218.

https://doi.org/10.1017/jfm.2025.283 Published online by Cambridge University Press

ERMANYUK, E.V. & GAVRILOV, N.V. 2002 Force on a body in a continuously stratified fluid. Part 1. Circular cylinder. *J. Fluid Mech.* **451**, 421–443.
ERMANYUK, E.V. & GAVRILOV, N.V. 2003 Force on a body in a continuously stratified fluid. Part 2. Sphere. *J. Fluid Mech.* **494**, 33–50.
FISH, F.E. & LAUDER, G.V. 2006 Passive and active flow control by swimming fishes and mammals. *Annu. Rev. Fluid Mech.* **38** (1), 193–224.
FLORYAN, D., VAN BUREN, T., ROWLEY, C.W. & SMITS, A.J. 2017 Scaling the propulsive performance of heaving and pitching foils. *J. Fluid Mech.* **822**, 386–397.
FLYNN, M.R., ONU, K. & SUTHERLAND, B.R. 2003 Internal wave excitation by a vertically oscillating sphere. *J. Fluid Mech.* **494**, 65–93.
GAZZOLA, M., ARGENTINA, M. & MAHADEVAN, L. 2014 Scaling macroscopic aquatic locomotion. *Nat. Phys.* **10** (10), 758–761.
GODOY-DIANA, R., AIDER, J.-L. & WESFREID, J.E. 2008 Transitions in the wake of a flapping foil. *Phys. Rev. E—Stat. Nonlinear Soft Matt. Phys.* **77** (1), 016308.
GUGLIELMINI, L. & BLONDEAUX, P. 2004 Propulsive efficiency of oscillating foils. *Eur. J. Mech.- B/Fluids* **23** (2), 255–278.
HANAZAKI, H., NAKAMURA, S. & YOSHIKAWA, H. 2015 Numerical simulation of jets generated by a sphere moving vertically in a stratified fluid. *J. Fluid Mech.* **765**, 424–451.
HOUGHTON, I.A., KOSEFF, J.R., MONISMITH, S.G. & DABIRI, J.O. 2018 Vertically migrating swimmers generate aggregation-scale eddies in a stratified column. *Nature* **556** (7702), 497–500.
HOWLAND, C.J., TAYLOR, J.R. & CAULFIELD, C.P. 2021 Shear-induced breaking of internal gravity waves. *J. Fluid Mech.* **921**, A24.
HURLEY, D.G. & KEADY, G. 1997 The generation of internal waves by vibrating elliptic cylinders. Part 2. Approximate viscous solution. *J. Fluid Mech.* **351**, 119–138.
ISOGAI, K., SHINMOTO, Y. & WATANABE, Y. 1999 Effects of dynamic stall on propulsive efficiency and thrust of flapping airfoil. *AIAA J.* **37** (10), 1145–1151.
IZRAELEVITZ, J.S. & TRIANTAFYLLOU, M.S. 2014 Adding in-line motion and model-based optimization offers exceptional force control authority in flapping foils. *J. Fluid Mech.* **742**, 5–34.
KANDEL, P. & DENG, J. 2022 Swimming in density-stratified fluid: study on a flapping foil. *Bioinspir. Biomim.* **17** (5), 055003.
LAM, T., VINCENT, L. & KANSO, E. 2019 Passive flight in density-stratified fluids. *J. Fluid Mech.* **860**, 200–223.
LIAO, J.C., BEAL, D.N., LAUDER, G.V. & TRIANTAFYLLOU, M.S. 2003 Fish exploiting vortices decrease muscle activity. *Science* **302** (5650), 1566–1569.
LIGHTHILL, M.J. 1967 On waves generated in dispersive systems by travelling forcing effects, with applications to the dynamics of rotating fluids. *J. Fluid Mech.* **27** (4), 725–752.
LOFQUIST, K.E.B. & PURTELL, L.P. 1984 Drag on a sphere moving horizontally through a stratified liquid. *J. Fluid Mech.* **148**, 271–284.
LUA, K.B., DASH, S.M., LIM, T.T. & YEO, K.S. 2016 On the thrust performance of a flapping two-dimensional elliptic airfoil in a forward flight. *J. Fluid. Struct.* **66**, 91–109.
MADISON, T.J., XIANG, X. & SPEDDING, G.R. 2022 Laboratory and numerical experiments on the near wake of a sphere in a stably stratified ambient. *J. Fluid Mech.* **933**, A12.
MAGNAUDET, J. & MERCIER, M.J. 2020 Particles, drops, and bubbles moving across sharp interfaces and stratified layers. *Annu. Rev. Fluid Mech.* **52** (1), 61–91.
MEUNIER, P. & SPEDDING, G.R. 2006 Stratified propelled wakes. *J. Fluid Mech.* **552**, 229–256.
MORE, R.V. & ARDEKANI, A.M. 2020 Motion of an inertial squirmer in a density stratified fluid. *J. Fluid Mech.* **905**, A9.
MORE, R.V. & ARDEKANI, A.M. 2023 Motion in stratified fluids. *Annu. Rev. Fluid Mech.* **55** (1), 157–192.
MORE, R.V., ARDEKANI, M.N., BRANDT, L. & ARDEKANI, A.M. 2021 Orientation instability of settling spheroids in a linearly density-stratified fluid. *J. Fluid Mech.* **929**, A7.
MUSCUTT, L.E., WEYMOUTH, G.D. & GANAPATHISUBRAMANI, B. 2017 Performance augmentation mechanism of in-line tandem flapping foils. *J. Fluid Mech.* **827**, 484–505.
NUDDS, R.L., JOHN, E.L., KEEN, A.N. & SHIELS, H.A. 2014 Rainbow trout provide the first experimental evidence for adherence to a distinct Strouhal number during animal oscillatory propulsion. *J. Expl Biol.* **217** (13), 2244–2249.
OKINO, S., AKIYAMA, S. & HANAZAKI, H. 2017 Velocity distribution around a sphere descending in a linearly stratified fluid. *J. Fluid Mech.* **826**, 759–780.
ORTIZ-TARIN, J.L., NIDHAN, S. & SARKAR, S. 2023 The high-Reynolds-number stratified wake of a slender body and its comparison with a bluff-body wake. *J. Fluid Mech.* **957**, A7.

https://doi.org/10.1017/jfm.2025.283 Published online by Cambridge University Press

PLATZER, M.F., JONES, K.D., YOUNG, J. & LAI, J.C.S. 2008 Flapping wing aerodynamics: progress and challenges. *AIAA J.* **46** (9), 2136–2149.
QUINN, D.B., MOORED, K.W., DEWEY, P.A. & SMITS, A.J. 2014 Unsteady propulsion near a solid boundary. *J. Fluid Mech.* **742**, 152–170.
READ, D.A., HOVER, F.S. & TRIANTAFYLLOU, M.S. 2003 Forces on oscillating foils for propulsion and maneuvering. *J. Fluid. Struct.* **17** (1), 163–183.
REHM, R.G. & RADT, H.S. 1975 Internal waves generated by a translating oscillating body. *J. Fluid Mech.* **68** (2), 235–258.
RILEY, J.J. & LELONG, M.-P. 2000 Fluid motions in the presence of strong stable stratification. *Annu. Rev. Fluid Mech.* **32** (1), 613–657.
ROHR, J.J. & FISH, F.E. 2004 Strouhal numbers and optimization of swimming by odontocete cetaceans. *J. Expl Biol.* **207** (10), 1633–1642.
ROZHDESTVENSKY K. 2022 Study of underwater and wave gliders on the basis of simplified mathematical models. *Appl. Sci.* **12** (7), 3465.
ROZHDESTVENSKY, K.V. & RYZHOV, V.A. 2003 Aerohydrodynamics of flapping-wing propulsors. *Prog. Aerosp. Sci.* **39** (8), 585–633.
SARPKAYA, T. 1983 Trailing vortices in homogeneous and density-stratified media. *J. Fluid Mech.* **136**, 85–109.
SCHLICHTING, H. & GERSTEN, K. 2016 *Boundary-Layer Theory*. Springer.
SCHNIPPER, T., ANDERSEN, A. & BOHR, T. 2009 Vortex wakes of a flapping foil. *J. Fluid Mech.* **633**, 411–423.
ŞENTÜRK, U. & SMITS, A.J. 2019 Reynolds number scaling of the propulsive performance of a pitching hydrofoil. *AIAA J.* **57** (7), 2663–2669.
SMITS, A.J. 2019 Undulatory and oscillatory swimming. *J. Fluid Mech.* **874**, P1.
SPALART, P.R. 1996 On the motion of laminar wing wakes in a stratified fluid. *J. Fluid Mech.* **327**, 139–160.
SPEDDING, G.R., BROWAND, F.K. & FINCHAM, A.M. 1996 Turbulence, similarity scaling and vortex geometry in the wake of a towed sphere in a stably stratified fluid. *J. Fluid Mech.* **314**, 53–103.
SPEDDING, G.R. 2014 Wake signature detection. *Annu. Rev. Fluid Mech.* **46** (1), 273–302.
STAQUET, C. & SOMMERIA, J. 2002 Internal gravity waves: from instabilities to turbulence. *Annu. Rev. Fluid Mech.* **34** (1), 559–593.
STEVENSON, T.N. & THOMAS, N.H. 1969 Two-dimensional internal waves generated by a travelling oscillating cylinder. *J. Fluid Mech.* **36** (3), 505–511.
SUTHERLAND, B.R. 2010 *Internal Gravity Waves*. Cambridge University Press.
TAYLOR, G.K. 2018 Simple scaling law predicts peak efficiency in oscillatory propulsion. *Proc. Natl Acad. Sc. USA* **115** (32), 8063–8065.
TAYLOR, G.K., NUDDS, R.L. & THOMAS, A.L.R. 2003 Flying and swimming animals cruise at a Strouhal number tuned for high power efficiency. *Nature* **425** (6959), 707–711.
TECHET, A.H. 2008 Propulsive performance of biologically inspired flapping foils at high Reynolds numbers. *J. Expl Biol.* **211** (2), 274–279.
THORPE, S.A. 2005 *The Turbulent Ocean*. Cambridge University Press.
TKACHEVA, L.A. 1995 Unsteady motion of a thin wing in a stratified fluid. *J. Appl. Mech. Tech. Phys.* **36** (6), 828–839.
TKACHEVA, L.A. 1998 Hydrodynamic characteristics of a wing in a stratified fluid near the bottom. *J. Appl. Mech. Tech. Phys.* **39** (1), 24–29.
TORRES, C.R., HANZAKI, H., OCHOA, J., CASTILLO, J. & VAN WOERT, M. 2000 Flow past a sphere moving vertically in a stratified diffusive fluid. *J. Fluid Mech* **417**, 211–236.
TRIANTAFYLLOU, G.S., TRIANTAFYLLOU, M.S. & GROSENBAUGH, M.A. 1993 Optimal thrust development in oscillating foils with application to fish propulsion. *J. Fluid. Struct.* **7** (2), 205–224.
TRIANTAFYLLOU, M.S. *et al.* 1991 Wake mechanics for thrust generation in oscillating foils. *Phys. Fluids A: Fluid Dyn.* **3** (12), 2835–2837.
TRIANTAFYLLOU, M.S., TRIANTAFYLLOU, G.S. & YUE, D.K.P. 2000 Hydrodynamics of fishlike swimming. *Annu. Rev. Fluid Mech.* **32** (1), 33–53.
TUNCER, I.H. & KAYA, M. 2005 Optimization of flapping airfoils for maximum thrust and propulsive efficiency. *AIAA J.* **43** (11), 2329–2336.
VAN BUREN, T., FLORYAN, D. & SMITS, A.J. 2019 Scaling and performance of simultaneously heaving and pitching foils. *AIAA J.* **57** (9), 3666–3677.
VERMA, S. & HEMMATI, A. 2022 Characterization of bifurcated dual vortex streets in the wake of an oscillating foil. *J. Fluid Mech.* **945**, A7.

https://doi.org/10.1017/jfm.2025.283 Published online by Cambridge University Press

VOISIN, B. 1994 Internal wave generation in uniformly stratified fluids. Part 2. Moving point sources. *J. Fluid Mech.* **261**, 333–374.

WANG, J., DENG, J., KANDEL, P. & SUN, L. 2023 Numerical study on the energy extraction performance by flapping foils in a density stratified flow. *J. Fluid. Struct.* **118**, 103865.

WANG, J., KANDEL, P. & DENG, J. 2024 High propulsive performance by an oscillating foil in a stratified fluid. *J. Fluid Mech.* **980**, A55.

WANG, S., WANG, J. & DENG, J. 2023 Effect of layer thickness for the bounce of a particle settling through a density transition layer. *Phys. Rev. E* **108** (6), 065108.

WANG, Z.J. 2000 Vortex shedding and frequency selection in flapping flight. *J. Fluid Mech.* **410**, 323–341.

WILLIAMSON, C.H.K. & ROSHKO, A. 1988 Vortex formation in the wake of an oscillating cylinder. *J. Fluid. Struct.* **2** (4), 355–381.

WU, T.Y. 2011 Fish swimming and bird/insect flight. *Annu. Rev. Fluid Mech.* **43** (1), 25–58.

YICK, K.Y., TORRES, C.R., PEACOCK, T. & STOCKER, R. 2009 Enhanced drag of a sphere settling in a stratified fluid at small Reynolds numbers. *J. Fluid Mech.* **632**, 49–68.

YOUNG, J. & LAI, J.C.S. 2007 Mechanisms influencing the efficiency of oscillating airfoil propulsion. *AIAA J.* **45** (7), 1695–1702.

ZHANG, J. 2017 Footprints of a flapping wing. *J. Fluid Mech.* **818**, 1–4.

ZHANG, J., MERCIER, M.J. & MAGNAUDET, J. 2019 Core mechanisms of drag enhancement on bodies settling in a stratified fluid. *J. Fluid Mech.* **875**, 622–656.

ZHOU, C. & LOW, K.H. 2011 Design and locomotion control of a biomimetic underwater vehicle with fin propulsion. *IEEE/ASME Trans. Mech.* **17** (1), 25–35.

ZHU, Q. 2007 Numerical simulation of a flapping foil with chordwise or spanwise flexibility. *AIAA J.* **45** (10), 2448–2457.

https://doi.org/10.1017/jfm.2025.283 Published online by Cambridge University Press